MASTERARBEIT

Titel der Masterarbeit

Structural and physicochemical characterization of

Basic Calcium Carbonate (BCC)

verfasst von

Manuel Ripken, BSc.

angestrebter akademischer Grad

Master of Science (MSc.)

Wien, 2015

Studienkennzahl lt. Studienblatt: A 066 815

Studienrichtung lt. Studienblatt: Erdwissenschaften

Betreuer: ao.Univ.-Prof. Dr. Christian L. Lengauer

Acknowledgement

Declaration

I hereby declare that this thesis contains no material, which has been submitted or accepted for an award of any other degree or diploma in any university or institution. To the best of my knowledge and belief, this thesis contains no material previously published by any other person except where acknowledgment has been made.

Vienna, April 2015

Manuel Ripken

Abstract

The best conditions for the storage of basic calcium carbonate (BCC) are dry environments. This is confirmed by pXRD analysis. At higher humidity conditions sample material transforms into vaterite-type calcium carbonate, while under a dry heating process it dehydrates and dehydroxylates to calcite-type calcium carbonate. Under ambient conditions the dehydrated modification does not convert to BCC, it also transforms to the vaterite-type calcium carbonate. High quality SEM images of a rapid converted vaterite-type calcium carbonate reveal imperfect pseudomorphs of vaterite after the platy BCC.

According to the observed and calculated weight losses of BCC and data from literature, one can state a mismatch with the reported chemical formula, which would require an overall weight loss of -14.9 wt% for $(OH)_2$ + $1.5H_2O$. As the observed weight loss is proven to be -12.3 wt%, which is very close to the calculated value for a monohydrate (-12.2 wt%), one can give for BCC the corrected chemical formula as $Ca_3(CO_3)_2(OH)_2 \cdot H_2O$.

The comparison of BCC and samples filtered from a slurry sample shows no differences with respect to the BCC phase. This was proven by pXRD- and IR-measurements. The slurry contains traces of calcite, vaterite and considerable amount of portlandite. Additional experiments were performed with the slurry sample. Three samples were filtered and each of them was washed with a different solvent. pXRD revealed only small differences between the treated samples.

Crystallography and the hitherto unknown structure of BCC were determined by analyzing pXRD patterns. BCC crystallizes monoclinic with space group *Pc*. The cell parameters of the pseudo-orthorhombic cell are $a = 8.661(1)$ Å, $b = 6.557(1)$ Å, $c = 7.078(1)$ Å, $\beta = 90.08(1)°$ and $V = 401.97(4)$ Å^3. The structure model shows similarities with those of portlandite, vaterite and hydromagnesite.

Zusammenfassung

Für die Aufbewahrung des basischen Kalziumkarbonats (BCC) eignen sich am besten trockene Bedingungen. Unter höherer Luftfeuchtigkeit findet eine Umwandlung des Materials in ein Vaterit-Typ Kalziumkarbonat statt. Wenn das BCC allerdings unter trockner Atmosphäre erhitzt wird, dehydriert und dehydroxiliert dieses in ein Kalzit-Typ Kalziumkarbonat. Aus der dehydrierten Modifikation entsteht kein BCC, sondern es wandelt sich ebenfalls in das Vaterit-Typ Kalziumkarbonat um. Diese Informationen wurden mit Pulver-Röntgendiffraktometrie (pXRD) bestätigt. Eine Elektronenmikroskopie-Aufnahme von diesem Vaterit-Typ Kalziumkarbonat zeigt eine Pseudomorphose von Vaterit nach BCC.

Aufgrund der erhaltenen und berechneten Gewichtsverluste des BCC und der Daten aus der Literatur, erhält man eine Diskrepanz in der chemischen Formel. Der Gewichtsverlust für $(OH)_2$ + $1.5H_2O$ sollte 14.9 wt% betragen. Der gemessene Gewichtsverlust von 12.3 wt% stimmt mit dem theoretischen Verlust des Monohydrats überein, somit kann die Formel als $Ca_3(CO_3)_2(OH)_2 \cdot H_2O$ angegeben werden.

Das Pulver wurde auch mit einer selbst filtrierten Probe aus einer Suspension verglichen. IR- und pXRD-Messungen zeigen keine Unterschiede der zwei Proben. Einzig Spuren von Kalzit, Vaterit und Portlandit sind in der Suspension enthalten. Außerdem wurden Versuche mit unterschiedlichen Waschlösungen nach der Filtration durchgeführt. Die Ergebnisse zeigen nur geringe Unterschiede.

Die Strukturbestimmung aus Pulverdaten ergibt eine monokline Elementarzelle mit der Raumgruppe *Pc* und den Zellparametern a=8.661(1) Å, b=6.557(1) Å, c=7.078(1) Å, β=90.08(1)° und V = 401.97(4) Å^3. Das Strukturmodell von BCC weist Ähnlichkeiten mit den Strukturen von Portlandit, Vaterit und Hydromagnesit auf.

Index of Contents:

1. Introduction

This study deals with the formation respectively precipitation of basic calcium carbonate (BCC) as well as its structural and physicochemical characterization, based on sample material supplied by commercial source. At the Department of Mineralogy and Crystallography at the University of Vienna, this BCC material was intended to be analyzed with powder X-ray diffraction (pXRD), thermal analyses (TA), chemical analyses, electron microscopic imaging (SEM) and spectroscopic methods. By using these techniques a structure model for BCC should be depicted.

Schimmel (1970) mentioned that chemical compounds of basic magnesium carbonate are known for a long time. In contrast to magnesium, the chemical compounds of calcium are missing. Some previous authors have discussed the existence of basic calcium carbonates, but Pietsch & Kotowski (1939) strongly doubted that fact. According to that, the interest in these compounds has been raised up.

The related basic magnesium carbonate is already known for a long time, and therefore it can be compared with each other. Literature shows a lot of different names for basic magnesium carbonate. Magnesium carbonicum and magnesia alba is very often used, however, magnesium subcarbonium is used rarely. The name of the two mineral within that group are artinite, $Mg_2(CO_3)(OH)_2 \cdot 3H_2O$ $(MgCO_3 \cdot Mg(OH)_2 \cdot 3H_2O)$ and hydromagnesite, $Mg_5(CO_3)_4(OH)_2 \cdot 4H_2O$ $(4MgCO_3 \cdot Mg(OH)_2 \cdot 4H_2O)$. Basic magnesium carbonate is important for the industry; it is used as a precursor for other magnesium based chemicals for plastic fillers, rubber and painting.

Relevant data and information of calcium carbonate were found in younger references, approximately since the nineties. Matushita et al. (1993-1995) and Grothe (Patent application 89122027.9, 1991) published the first conditions for the formation of BCC as well as the first structural and physicochemical properties. The given chemical formula is $Ca_3(CO_3)_2(OH)_2 \cdot 2H_2O$ or $2CaCO_3 \cdot Ca(OH)_2 \cdot 2H_2O$.

Furthermore, this study contains the results and interpretation of the investigations on basic calcium carbonate (BCC). This information is used to understand the physicochemical properties. In addition to the stability of this carbonate, the chemical composition and the thermal behavior have been analyzed. The structure determination and description was not covered in this study.

Previous literature reviews contain only limited data of BCC's properties. Therefore, a lot of different methods were used to achieve more information. There are several sources, which deal with the thermal properties of BCC. Matsushita et al. (1993b, 1995) published detailed descriptions of TG and DTA measurements, which were compared with the results of this study.

The original sample was compared with some other samples, which were prepared from a slurry sample. The difference between these samples was the washing treatment step after the filtration of the slurry. Moreover the conversion product of BCC-ori, which is a vaterite-type calcium carbonate, has been analyzed and compared with the precipitate.

A very interesting task was the structure solution. A structural model was derived and consecutively refined. The results were interpreted, evaluated and compared with the crystal structure from vaterite, portlandite and hydromagnesite. Portlandite is the starting material and vaterite the conversion product of BCC under ambient conditions and one can assume similarities in the crystal structures. Hydromagnesite is a mineral of the group of the basic magnesium carbonate and has a comparable formula and structure. A disadvantage is that only powder samples are available. Consequently, it is impossible to locate hydrogen atoms. Oxygen atoms with a possible hydrogen bond were determined with the bond valence parameters after Breese and O'Keeffe (1991).

2. Literature review

2.1. Synthesis of basic calcium carbonate

Generally the same principle is described for the synthesis of BCC in all references. The following reaction equation can be found in several papers and abstracts:

$$3Ca(OH)_2 + 2CO_2 \rightarrow Ca_3(OH)_2(CO_3)_2 + 2H_2O$$

Important parameters for the precipitation of BCC are the concentration of calcium hydroxide (portlandite), the reaction temperature and the flow rate of CO_2.

Schimmel (1970) reported the procedure to obtain BCC: The starting material was an aqueous suspension of portlandite. Some special equipment was used to blow CO_2 into this suspension at 20 to 40 °C. Subsequently the BCC precipitated. The results of these experiments showed that this compound was metastable and decayed slowly to calcite and portlandite. Nevertheless, there is a demand in industry that these products are stable for a longer period of time. According to Grothe (1991) the carbonation process must be stopped, if the molar ratio of calcium and carbonate is 3:2 or 6:5 at temperatures from 2 to 50 °C. The patent also lists the different types of BCC. Depending on the initial temperature and concentration of the portlandite suspension different particle morphologies can be generated; ranging from platelet over fibers to large rhombohedra of BCC. Other properties can be obtained by further additives. One example: A CaO-suspension, with a concentration of 70 gl^{-1}, was carbonated at 10 °C with a CO_2-Air mixture (40:60). If the molar ratio of calcium and carbonate is 3:2 or 6:5, the process is finished.

Subsequently, Matasushita et al. (1993), performed experiments to achieve information of the pyrolysis of BCC. Therefore 2000 grams of a portlandite suspension (5 wt%) were carbonated by passing CO_2 with a flow rate of 340 $mlmin^{-1}$ for 60 min at 15 °C. This product was filtered, washed with acetone and dried for 24 hours. They analyzed this BCC by means of pXRD to derive basic structural information.

Ahn et al. (2003) published experimental conditions for the synthesis of platelet-like BCC. They tested various combinations of the synthesis parameters, i.e. concentration of $Ca(OH)_2$-suspension, reaction temperature and CO_2-flow rate (Table 1). The product exhibited good physical properties as a pigment for drawing papers.

Concentration of Ca(OH)$_2$ slurry [wt%]	React. temp. [°C]	CO$_2$ flow rate [mlmin^{-1}]	Synthesis
5.0	10	100	O
		150, 200, 250	X
	15	100, 150, 200	O
		250	X
	20	100, 150, 200, 250	X
4.0	10	100	O
		150, 200, 250	X
3.0	15	100, 150, 200, 250	X

Table 1: Experimental conditions of the synthesis of BCC, (O = BCC could be formed, X=BCC was not formed), after Ahn et al. (2003).

Further tests were performed by Ryu et al. (2007); they synthesized BCC under various basic conditions. Especially, the pH was controlled constantly with NH$_4$OH and KOH solutions during the carbonation reaction. Each sample was analyzed with pXRD, SEM and ICP-AES. One can conclude that the effect of the additives to control pH is larger than the reaction pH.

Ahn et al. (2011) and Yamada et. al. (1991) also prepared BCC under the same conditions than the authors before.

2.2. Synthesis of basic magnesium carbonate

Contrary to BCC the magnesium carbonate has been known for a long time. Pietsch (1939) has already described the formation of basic magnesium carbonate. Liu et al. (2011) shows this in a flow chart (Figure 1). There are two types, the light-burned (caustered) and the sintered type magnesia. The same amount of sodium carbonate and magnesium sulphate is mixed with water, both solved at approximately 70 °C. Under constant stirring (10 min.) the reaction mixture is heated to 95 °C, afterwards the precipitation is filtered and dried. Depending on the reaction temperature and the molar ratios of the starting materials, different products of basic magnesium carbonate are generated. The formation of basic calcium carbonate can only be assumed, because evidences were missing.
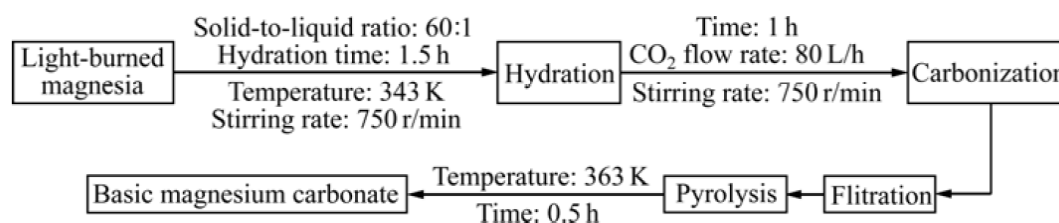

Figure 1: Preparation flow chart of basic magnesium carbonate, from Liu et al. (2011)

2.3. Structural and physicochemical characterization

According to Matsushita et al. (1993a) it was proved that BCC crystallizes with orthorhombic symmetry with cell parameters of a=7.094 Å, b=8.627 Å and c=6.558 Å. The system was determined by analyzing pXRD patterns. Moreover the decomposition process of BCC in water at 40-80 °C was investigated by means of pXRD and SEM.

Figure 2 shows the pXRD patterns of the products of decomposition of BCC at 60 °C. After 30 min the decomposition begins and small peaks can be assigned to calcite, aragonite and portlandite. Over time the decomposition process increased, as long as after 107 min BCC disappeared.

Figure 3 plots the weight fractions of BCC, calcite, aragonite and portlandite during the decomposition process at 60 °C. After 60 minutes the amount of BCC decreased stronger. At the end of the reaction the amount of calcite and aragonite became nearly equal.

Additionally, the fractions were analyzed with SEM. The BCC particles became small and fine. With onward decomposition needle-like products were observed and the particles became larger.
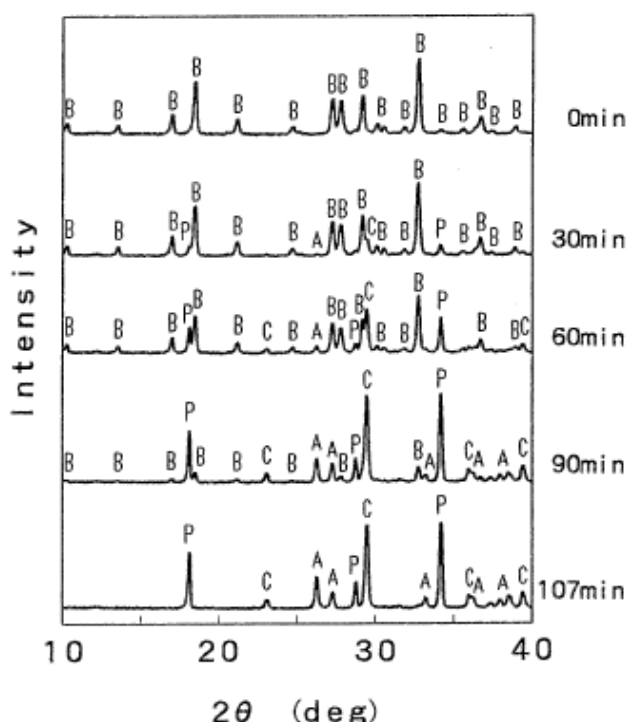

Figure 2: pXRD of BCC at 60 °C; (B=BCC, P=Ca(OH)$_2$, C=calcite, A=aragonite), from Matsushita et al. (1993a)
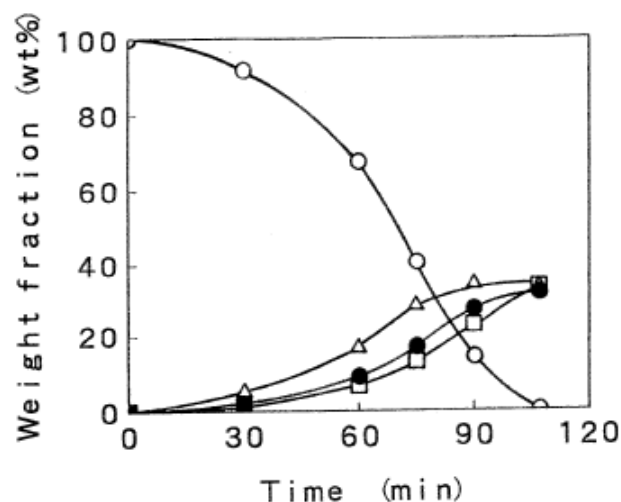

Figure 3: Weight fractions of components in decomposition process at 60 °C (○=BCC, ●=Ca(OH)$_2$, Δ=calcite, □=aragonite), from Matsushita et al.(1993a)
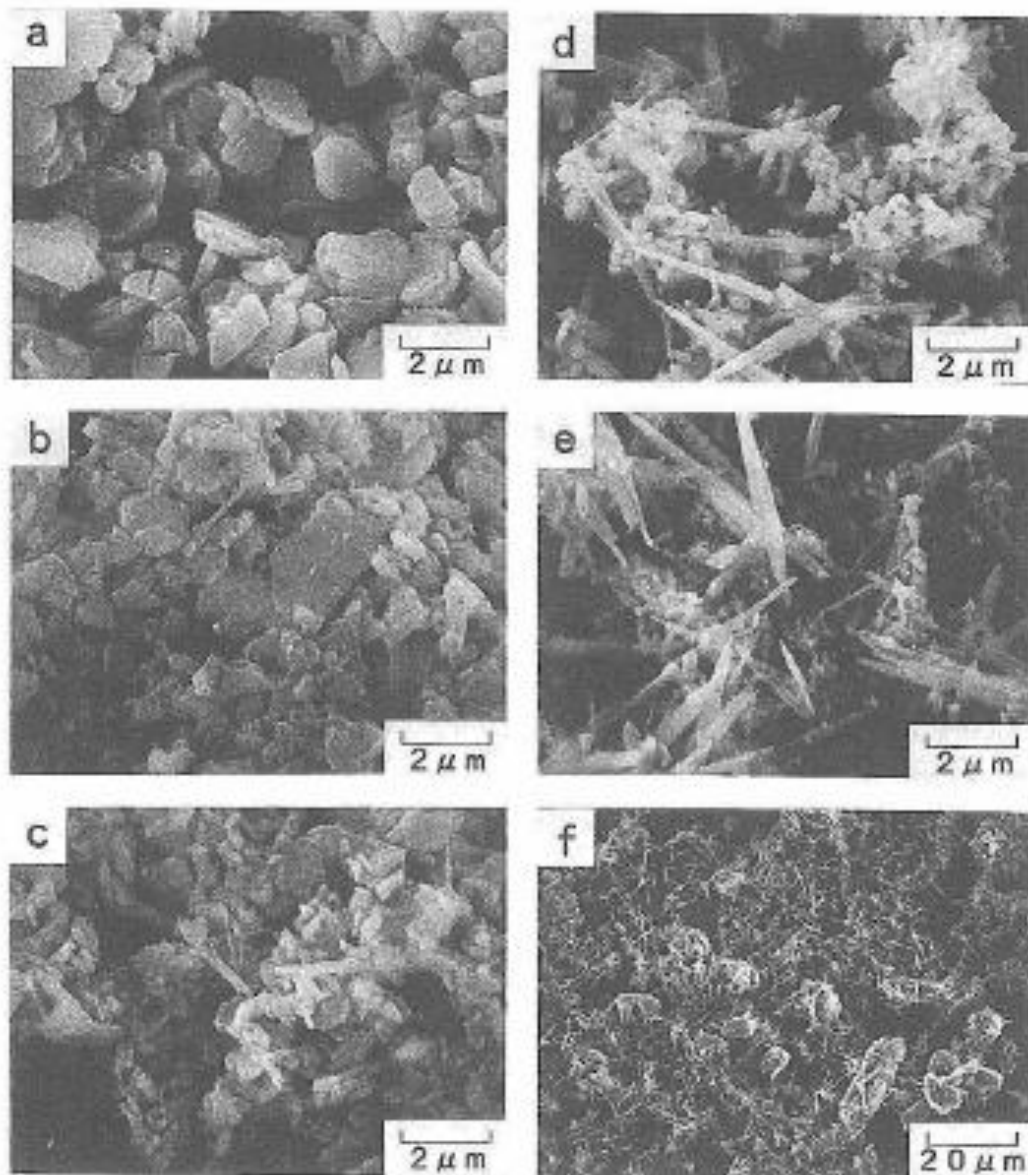
Figure 4: SEM photographs of products of decomposition of BCC at 60 °C, a=raw material, b=30 min, c=60 min, d= 75 min, e,f=107 min, from Matsushita et al., (1993a)

Figure 4 shows the pictures of the specimens in the course of decomposition at 60 °C. During the transformation progress the particles became smaller and needle like particles were observed. After 107 min very fine (0.2 µm) and huge particles (5-10 µm) can be seen.

Grothe (1991) produced different products of BCC under several conditions. The exact initial conditions can be found in the cited European patents. The results were a mix out of many different forms of BCC, documented by drawings of 12 BCC products.

Another publication from Matsushita et al. (1993b) deals with the thermal behavior of BCC using thermogravimetry (TG) and differential thermal analysis (DTA). In their study three endothermic peaks were obtained, which correspond to the three decreasing steps in the TG curve presented in Figure 5 and 6.
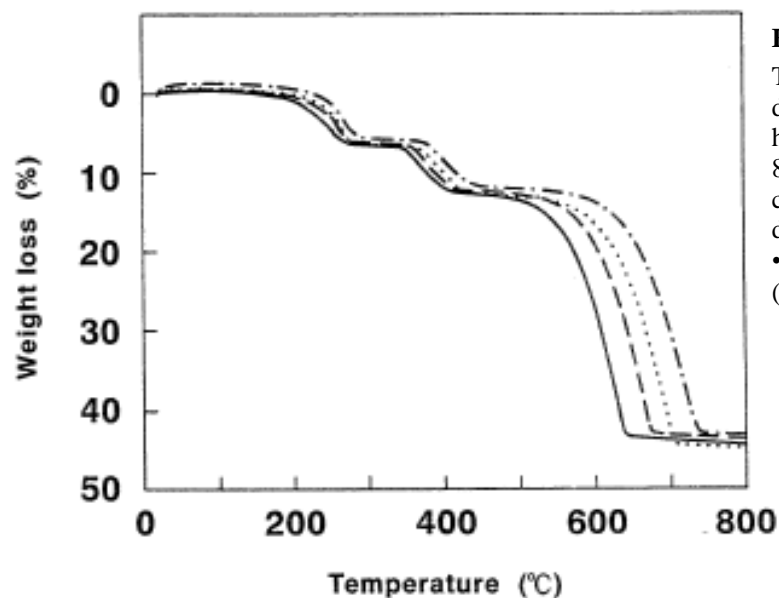

Figure 5: TG curves for thermal decomposition of BCC at various heating rates. (Specimen weight: 8 mg, Atmosphere: N_2 at 100 cm^3min^{-1}, Heating rate in $degmin^{-1}$; __:2, ----:5, •••:10, •-•-•-: 20), from Matsushita et al. (1993b)
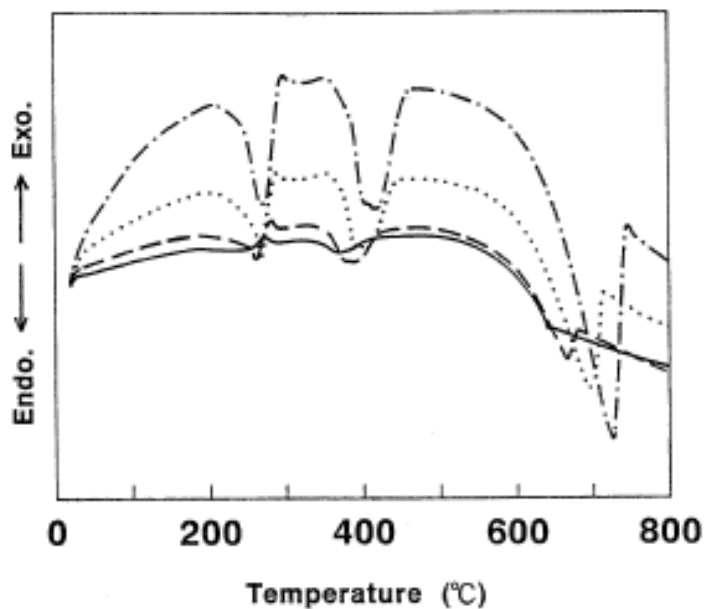

Figure 6: DTA curves for thermal decomposition of BCC at various heating rates. (Specimen weight: 8 mg, Atmosphere: N_2 at 100 cm^3min^{-1}, Heating rate in $degmin^{-1}$; __:2, ----:5, •••:10, •-•-•-:20), from Matsushita et al. (1993b)
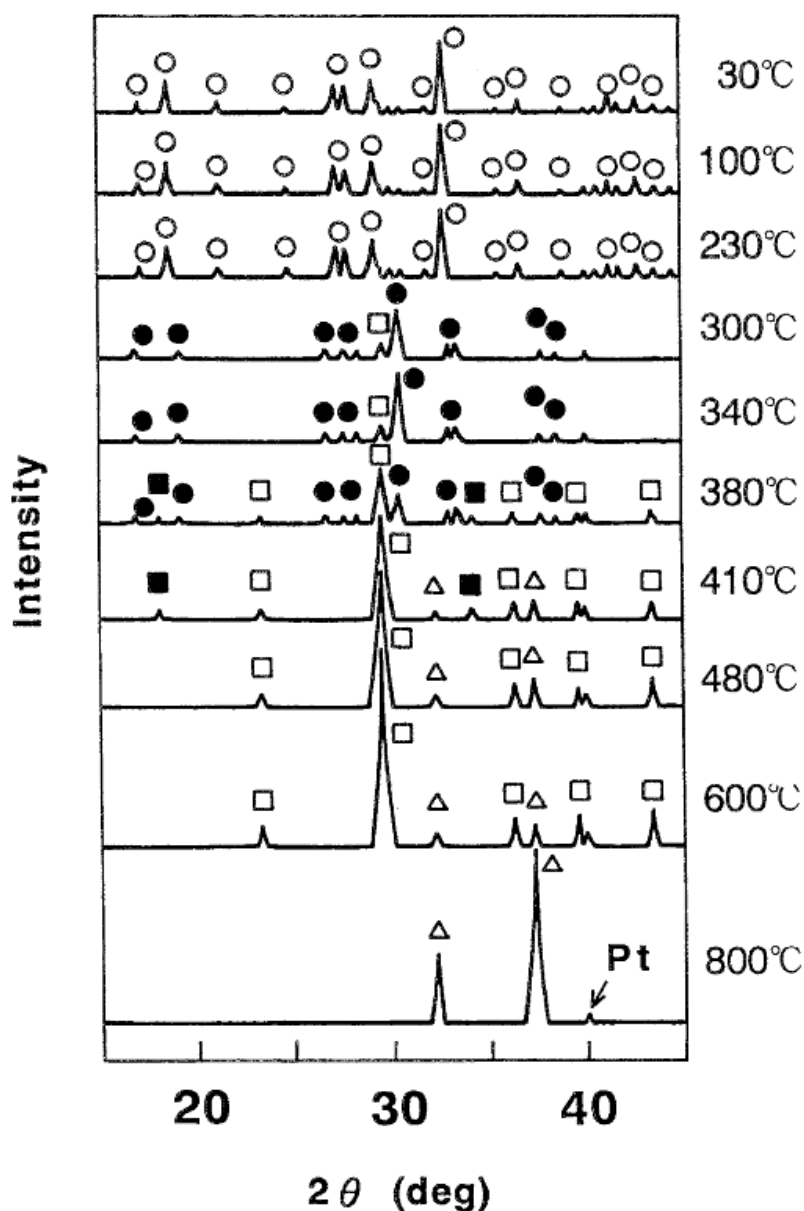
Figure 7: In situ pXRD patterns for BCC and its decomposition products. (Heating rate: 10 degmin^{-1}, Scan speed: 20 degmin^{-1}, Atmosphere: N_2 at 1000 cm^{3}min^{-1}, ($\circ$=BCC, $\bullet$=BCC-anhydride, Δ=CaO, $\square$=calcite, $\blacksquare$=Ca(OH)$_2$), from Matsushita et al.(1993b)

The first endothermic peak is a dehydration process of BCC at approximately 230 °C. Hereby, an unknown BCC anhydride was formed. The second one at 400 °C was the decomposition of BCC anhydride with the formation of calcite and portlandite. The third endothermic process corresponded to the formation of CaO. For confirmation infrared absorption spectra, TG-MS measurement and SEM pictures were obtained. Additionally, high temperature pXRD was performed.

The results of the decomposition process of BCC under air were compared with the existing results under N_2 atmosphere. The small amount of CO_2 induced a carbonation of intermediate products. Matsushita et al. (1995) presented the results of the TG and DTA curves under air- and N_2-atmosphere as well as the pXRD patterns.
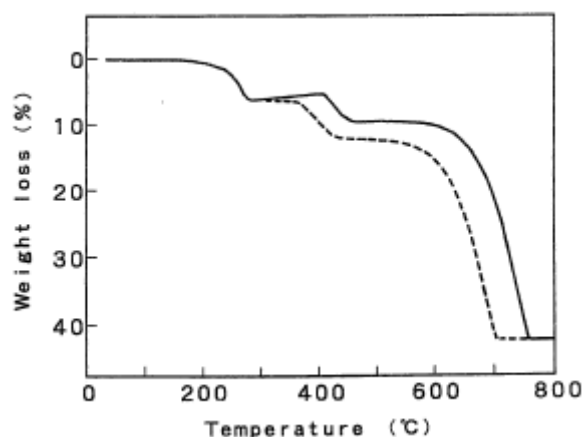

Figure 8:

TG curves for thermal decomposition of BCC, (Specimen weight: 8 mg, heating rate: 10 degmin[-1] Atmosphere: __:air, - - -:N_2), from Matsushita et al. (1995)

Figure 9:

DTA curves for thermal decomposition of BCC, (Specimen weight: 8 mg, heating rate: 10 degmin[-1] Atmosphere: __:air, - - - :N_2), from Matsushita et al. (1995)
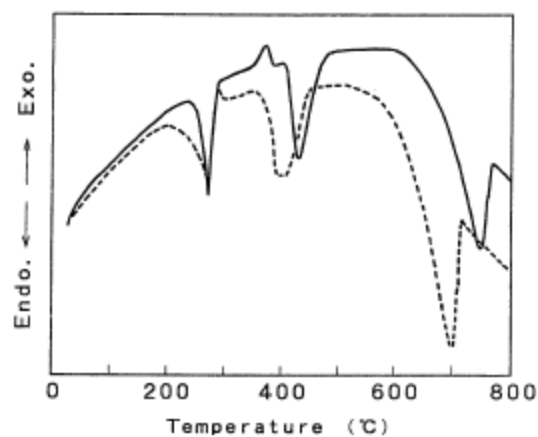
Around 370 °C the DTA curve figured out an exothermic peak, which was attributed to the crystallization of $CaCO_3$. Under N_2-atmosphere this peak is missing. Furthermore, the authors described the common observation that the peaks of the endothermic and exothermic processes were shifted to higher temperatures, if the heating rate is increased. The same statement was applied to the decomposition of $Ca(OH)_2$ and subsequently to $CaCO_3$. These shifts were explained by the effect of carbon dioxide.

In 2003 a team from the Korea Institute of Geosciences and Mineral Resources and School of Materials Sciences & Engineering in Seoul worked on a study, where the optimum experimental conditions of pH, reaction temperature and electric conductivity were examined. (Ahn et al. (2003))

After presenting the experimental conditions of the synthesis of BCC (Table 1), the authors dealt with the time related change of electrical conductivity during the whole carbonation process. The starting parameters were a slurry of $Ca(OH)_2$ with 5 wt%, an initial temperature of 15 °C and a CO_2 flow rate of 150 mlmin^{-1}. The following Figure shows the electrical conductivity and pH changes during the carbonation process.
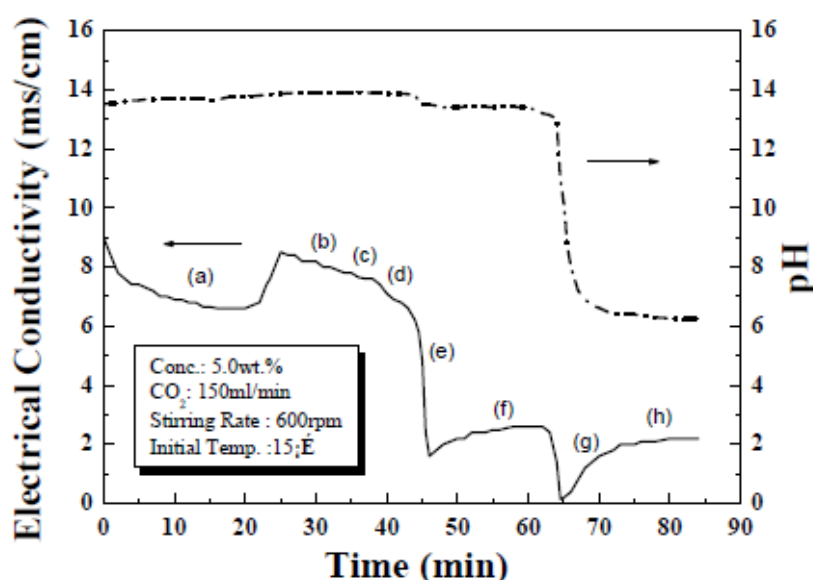

Figure 10: Electrical conductivity and pH changes during carbonation of 5 wt% $Ca(OH)_2$ slurry at 15 °C, __:Conductivity:, •-•-•-:pH, from Ahn et al. (2003)

For electrical conductivity a primary drop occurred in the beginning and after 20 minutes reaction time a primary rise occurred. At this time the pH of the reaction was hardly changed. After 44 minutes the electric conductivity decreased to 1.4 mScm^{-1}. At that time the formation of BCC was completed and the process of decomposition to calcite started. When 65 minutes had passed pH dropped down to 6, which was an indicator for the completed reaction. During this reaction eight samples (a-h) were extracted for a pXRD analysis. Ahn et al. (2003) indicated the pXRD patterns of each point in the electric conductivity curve (Figure 11). These analyses prove that the decomposition began at point (e) after 44 minutes reaction time. At this time the main peak of calcite began to grow. At point (g) BCC was completely decomposed.
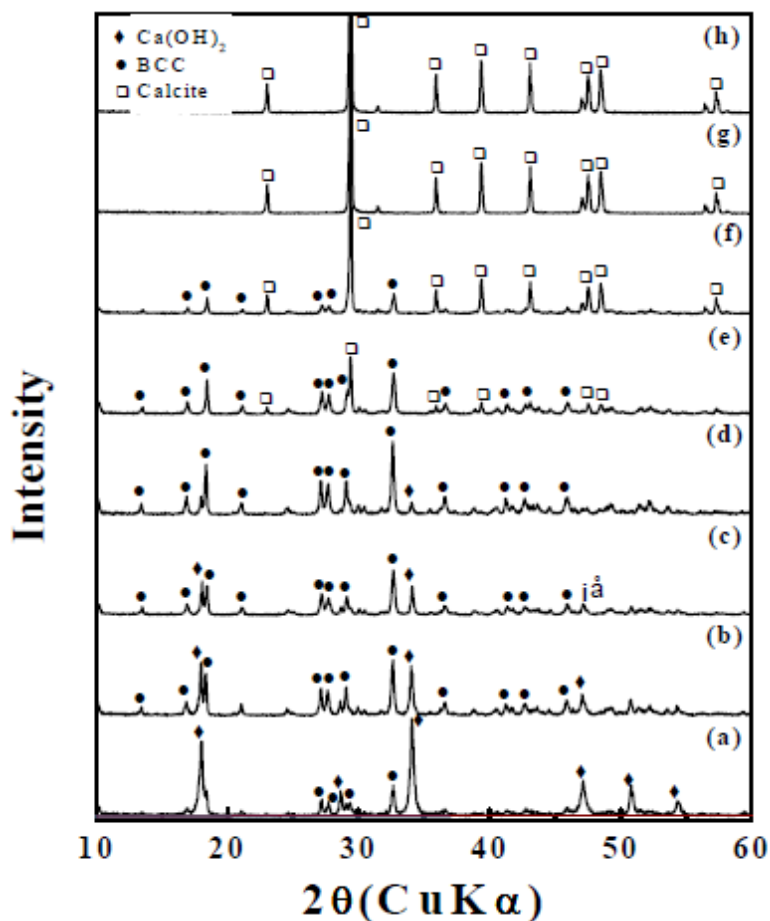
Figure 11: pXRD patterns of each point in electric conductivity curve, from Ahn et al. (2003)
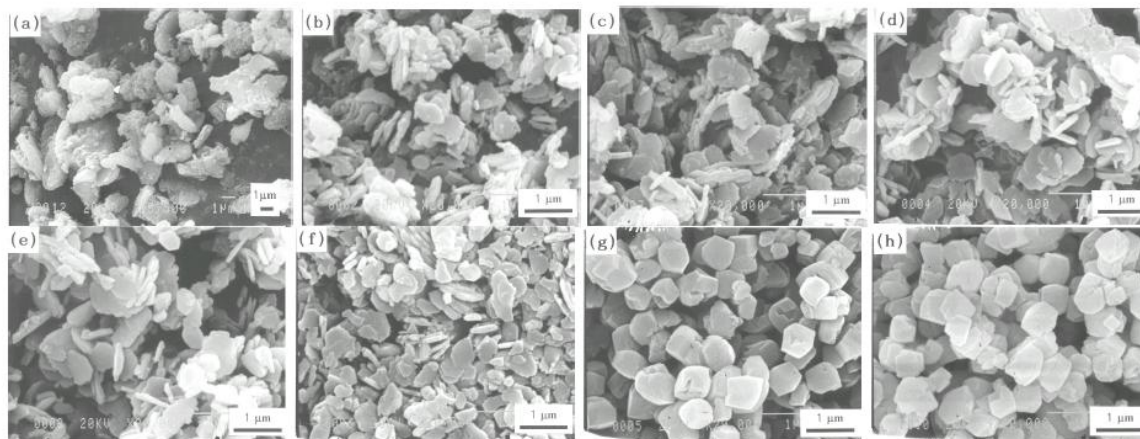

Figure 12: SEM photographs of calcium carbonate during carbonation process, from Ahn et al.(2003)

A related paper from Ryu et al. (2007) included dependencies of pH and conductivity of the solution controlled with NH_4OH and KOH. The precipitate was also analyzed with pXRD and the particles were measured with SEM. But Ryu et al. (2007), who dealt with the synthesis of BCC, did not include physicochemical properties of the products.

2.4. Characterization of basic magnesium carbonate

After the preparation of basic magnesium carbonate in accordance to the workflow of Figure 1, Liu et al. (2011) analyzed it with pXRD and observed the thermal decomposition. The result was a monoclinic unit cell with the parameters a=10.11 Å, b=8.94 Å, c=8.38 Å and β=114.58°.
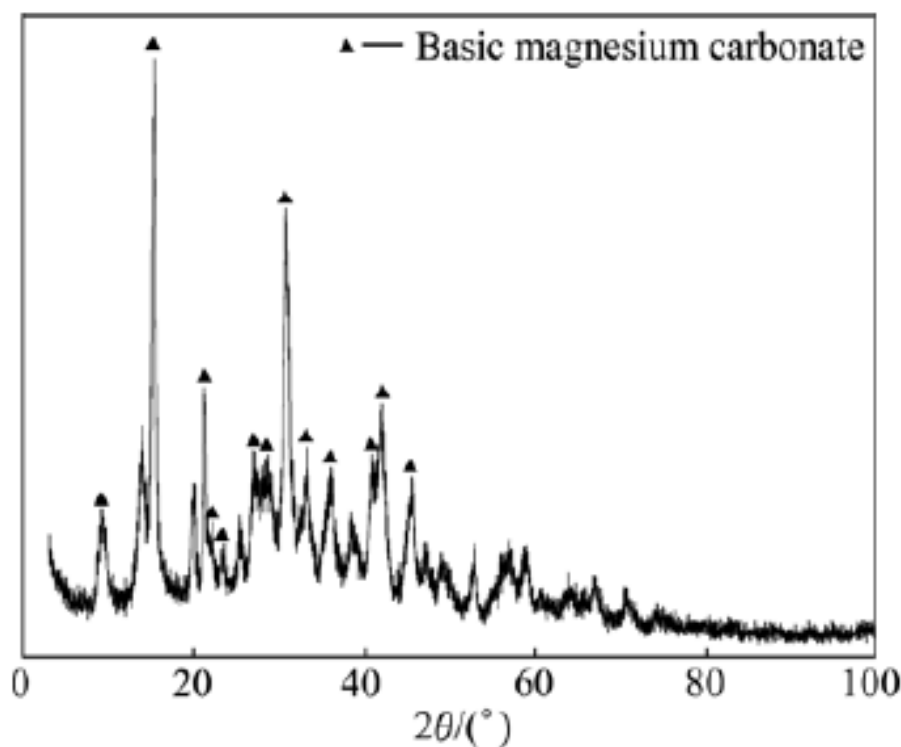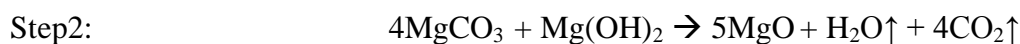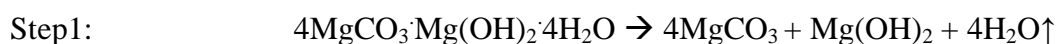

Figure 13:   pXRD pattern of basic magnesium carbonate, from Liu et al. (2011)

In the thermal decomposition process there were two steps of weight loss. The first step indicated the water loss in the range of 150-300 °C. The weight loss was about -15 wt%. The second decomposition step was in the range of 300-550 °C with a weight loss of -57 wt%.

At the end of this process basic magnesium carbonate was completely decomposed to magnesium oxide, water and carbon dioxide.

Step1: $4MgCO_3 \cdot Mg(OH)_2 \cdot 4H_2O \rightarrow 4MgCO_3 + Mg(OH)_2 + 4H_2O\uparrow$

Step2: $4MgCO_3 + Mg(OH)_2 \rightarrow 5MgO + H_2O\uparrow + 4CO_2\uparrow$

The associated endothermic peaks occurred at 235 °C (508 K) and 456 °C (729 K), shown in Figure 14.
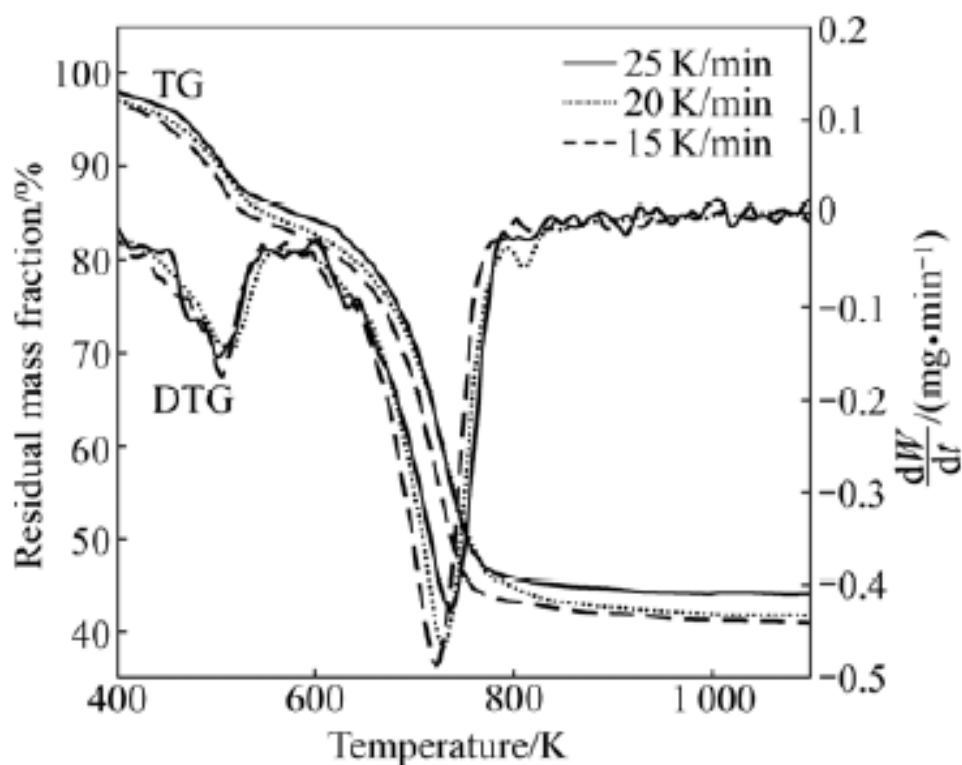
Figure 14: TG and DTG curves of basic magnesium carbonate, thermal decomposition at different heating rates, from Liu et al. (2011)

Pietsch (1939) described the physical and chemical properties of basic magnesium carbonate. Although the literature is old these values are still in use as reference.

physical properties	
density	$1.9 - 2.19$ gcm^{-3}
hardness (Mohs)	3-4
specific heat capacity	1.027 Jg^{-1}K^{-1}
refractive index	$1.515 - 1.530$
chemical properties	
to light	no reduction of CO_2
heating	hydromagnesite: two maxima, release of CO_2 at 300 °C and 560 °C
to air and water	hygroscopic, during heating in water → release of CO_2
solubility at 25 °C	$0.1 - 0.4$ gl^{-1}

Table 2: Physical and chemical properties of basic magnesium carbonate, after Pietsch (1939)

2.5. Application

Ryuichi et al. (1991) obtained a coated paper, which has two layers consisting of an undercoat and a top coat layer. This undercoat layer contained BCC as the pigment component with a BCC amount of about 20 wt%.

The carbonate, which was manufactured by Grothe (1991), showed resistant properties and is now available for further industrial processing and usage. Because of quality, the products are particularly suitable for use in paper manufacturing, emulsion paints, filler materials and synthetic resin. Especially flaky forms of BCC have a very strong coverage power.

3. Sample material

In this study synthesized BCC-type calcium carbonate was used for the investigation of the physicochemical characterization. Differences occurred in the post-treatment of the BCC, which was prepared from the slurry sample. In addition, a further modification of dehydrated BCC and the conversion product, i.e. the vaterite-type calcium carbonate, has been investigated.

BCC-syn:

The original precipitated BCC sample F31546.

BCC-slurry:

It was prepared from the slurry sample F31547: 50 ml of the slurry was filtered, washed with ethanol and then dried at 110 °C.

Figure 15: Sample BCC-syn.

Figure 16: Sample BCC-slurry.

BCC-ori:

A further precipitated BCC sample F8238, which was used for the structure determination.

BCC-dehy:

BCC-syn was dehydrated by exposing it to a temperature of 225 °C for 24 hours according to the results of preliminary TG measurements.

Vaterite-type calcium carbonate:

It is the stable conversion product of the original precipitated BCC. Under high to ambient humidity BCC-syn converted to a vaterite-type calcium carbonate, the hexagonal polymorph of calcium carbonate.

Sample B1:

20 ml BCC-slurry and 20 ml ethanol were filtered simultaneously. Afterwards the sample was washed with ethanol and dried at 110 °C.

Sample B2:

50 ml BCC-slurry was filtered, washed with 1 M NaOH solution and dried at 110 °C.

Sample B3:

50 ml BCC-slurry was filtered, washed with distilled water and dried at 110 °C.

	BCC	SLU	DHY	VAT	B1	B2	B3
pXRD	o	o	o	o	o	o	o
IR	o	o	o	o			
Raman	o		o	o	o	o	o
TG	o						
DSC	o	o					
CHNS	o						
TG-MS	o						

Table 3: Table shows which methods are used to investigate the different samples (BCC: BCC-ori; SLU: BCC-slurry; DHY: BCC-dehy; VAT: vaterite-type calcium carbonate from BCC-syn; B1-3: different prepared BCC- slurry samples).

4. Methods

X-ray diffraction and spectroscopic techniques were used as well as thermal analysis to determine the behavior of this precipitated BCC-carbonate. In addition a CHNS-analysis was performed. For a cross reference see Table 3.

Following methods are used:

- Scanning electron microscopy (SEM)
- Powder X-ray diffractometry (pXRD)
- Raman spectroscopy
- Infrared spectroscopy (IR)
- Thermogravimetry (TG)
- Evolved gas mass spectrometry (TG-EGA-MS)
- Differential scanning calorimetry (DSC)
- CHNS-analysis

4.1. Scanning electron microscopy (SEM)

The recordings were performed with a FEG REM Zeiss DSM 982 Gemini with a SE-detector (5KV).

4.2. Powder X-ray diffractometry (pXRD)

4.2.1. Ambient & non-ambient behavior

For qualitative measurements a Philips X'Pert pXRD with θ-2θ goniometer, scintillation counter and 21 position sample changer was used. A scan range from 5 to 65 °2θ and a step width of 0.02 °2θ was selected. The measurement duration is about 55 minutes. The samples were prepared on a low-background silicon plate. The current was 40 mA and the voltage 40 kV. For the non-ambient measurements a Bruker D8-Advanced θ-θ diffractometer with an Anton Paar XRX900 reaction chamber and a LynxEye position sensitive detector was used applying He (5.0, Messer) and evacuated conditions (<0.05 hPa) in the temperature range from 25 to 650 °C with dT-intervals of 25 °C. Measured range was 4 to 75 °2θ with an overall measurement time of 60 min and 5 min for equilibration prior to data collection at each temperature step.

4.2.2. Structure determination

The mineralogical composition was determined by using a Bruker D8 X-ray diffractometer, equipped with a position sensitive device (PSD) LynxEye detector system. Peak identification of given mineral phases was done by using the program DiffracPlus-EVA and the ICDD mineral data base. To determine the modal mineral composition semi quantitative Rietveld refinement calculations of the analyzed pXRD patterns were done by using the program TOPAS, applying the fundamental parameter approach. pXRD measurement conditions were 40 kV, by using a variable 6 mm divergence slit width, 2 angle: 4-70°, step size: 0.008° and time/step 0.2 seconds, which yielded a total measurement time for each sample of 30 minutes. All samples were prepared as powdered samples and measured with sample rotation.

For the following refinement, a starting structure solution model was used. This solution was generated with "simulated annealing".

4.2.3. Structure refinement

The disadvantage of the powder method is that the diffraction peaks grossly overlap, thereby the correctly determination of the structure is prevented. The Rietveld method creates a virtual separation of these overlapping peaks, which allow a better determination of the structure. Point by point reflex contributions were calculated in small diffraction angle steps (0.02 °2θ). The method forms a peak function with the individual mass points and calculates a diffractogram. This was compared with the observed diffractogram. Consecutively parameters were modified and a new refinement was started.

4.3. Spectroscopy

4.3.1. Infrared Spectroscopy (IR)

For infrared spectroscopy a Bruker Tensor 27 infrared spectrometer was used. For the measurements 32 Scans were recorded in a range from 4000 to 370 cm^{-1}. The solid sample powder was prepared on an attenuated total reflectance (ATR) diamond system. For comparison an analysis with a KBr-pellet was recorded.

4.3.2. Raman spectroscopy

The analysis was performed with a Horiba Jobin Yvon LabRAM-HR 800 spectrometer. The system was used with a 633 nm laser excitation and spectra in the range of 4000 to 60 cm^{-1} were recorded. For a further experiment the Linkam FTIR600 heating/cooling stage equipped with thin glass windows and electronic temperature control was used.

4.4. Thermal analyses

4.4.1. Thermogravimetry (TG)

A Mettler SDTA851e with sample charger was used. The BCC samples were heated from 25 to 900 °C with a heating rate of 5 °Cmin^{-1}. N$_2$ (5.0, Messer) was used as inert purge gas.

4.4.2. Evolved gas mass spectrometry (TG-EGA-MS)

Sample material was analyzed with a TG-EGA-MS system at the University of Innsbruck. The measurements were performed with a Setaram SETSYS Evolution-2400 TG-DTA system extended with a Pfeiffer Omnistar QMS200 mass-spectrometer. The samples were heated from 30 to 900 °C with a heating rate of 10 °Cmin^{-1}. He (5.0, Air Liquide) was used as carrier gas.

4.4.3. Differential Scanning calorimetry (DSC)

For these measurements a Mettler DSC821e with a LN2 cooling unit was used. The precipitate was exposed to an isothermic-dynamic-isotherm temperature program (0 °C: 5 min, 0-550 °C: 10 °Cmin^{-1}, 550 °C: 5 min). N$_2$ (5.0, Messer) was used as inert purge gas.

4.5. CHNS-analysis

The qualitative amount of carbon, hydrogen, nitrogen and sulfur was determined with the ELEMENTAR vario MACRO analyzer. Two more measurements were recorded with the LECO RC612 to determine the carbon content.

5. Results

5.1. Scanning electron microscopy (SEM)

The following Figures 17.a-b display images for BCC-syn and its vaterite-type calcium carbonate conversion product with scanning electron microscopy. The vaterite-type material resembles the platy habit of BCC-syn, however, as there is a difference in the cell volumes of BCC (~402 A^3) and vaterite (~125 A^3) the pseudomorphs are imperfect, probably pending on the transformation conditions.
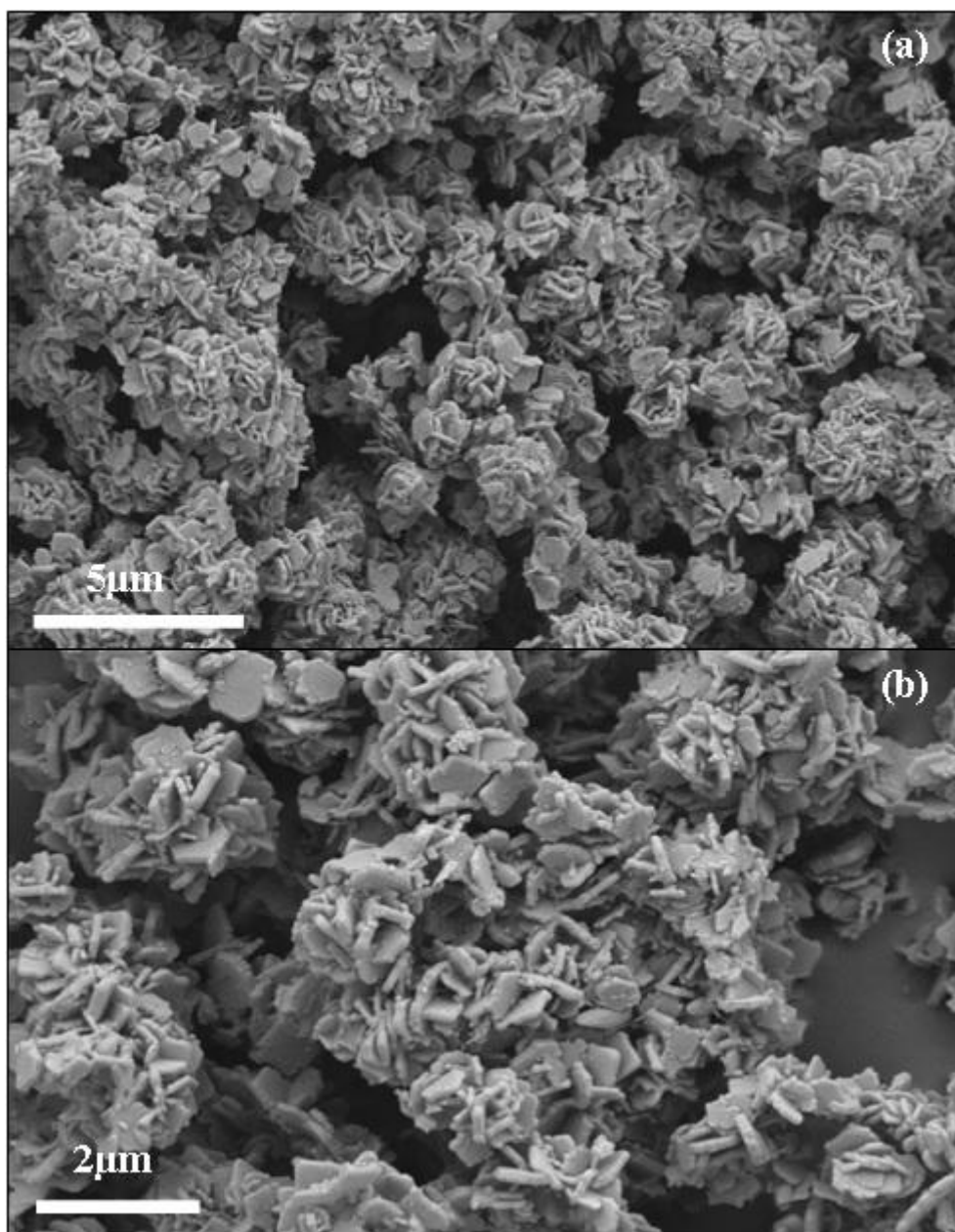

Figure 17.a, b: SEM images of BCC-syn (a,b)
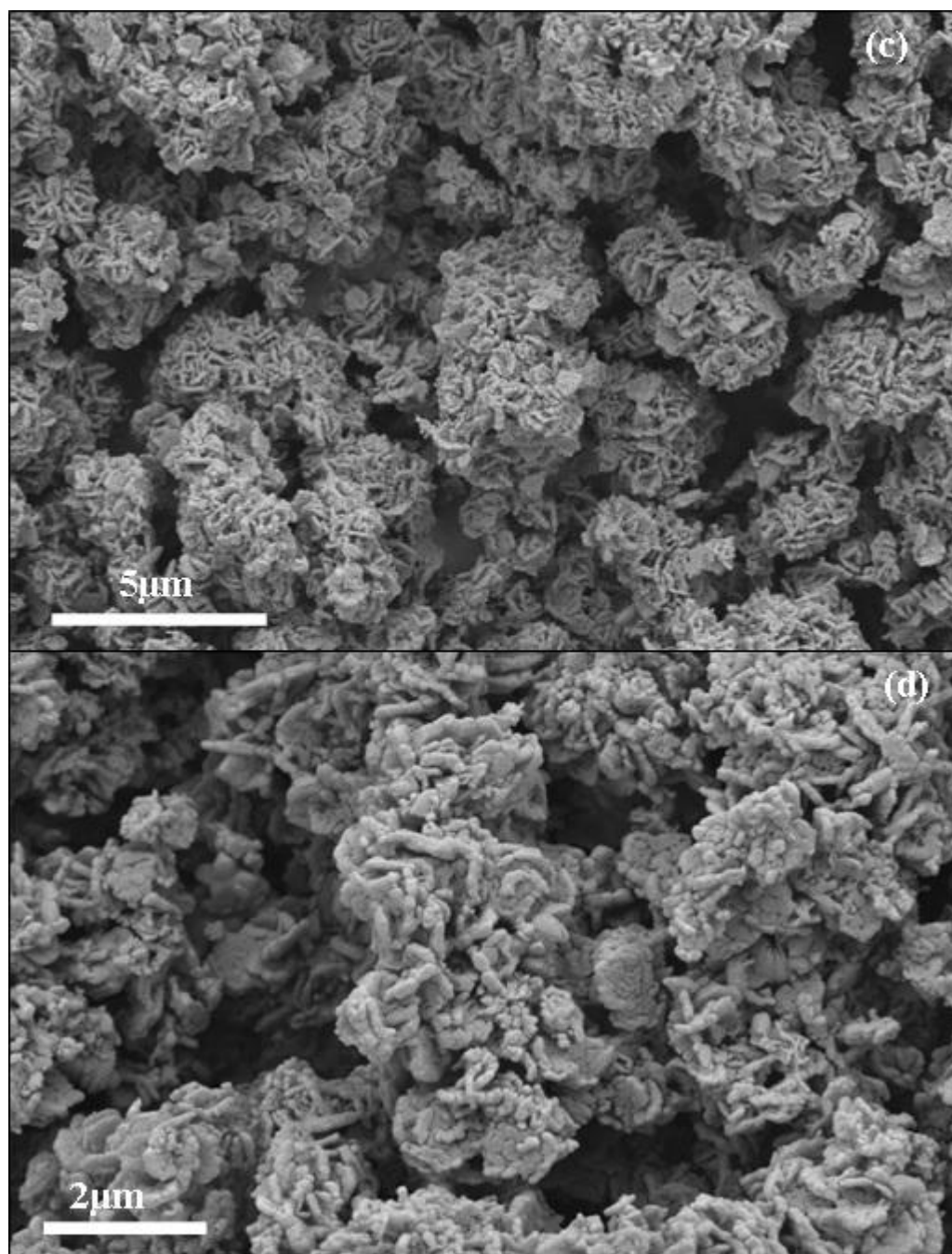
Figure 17.c,d: SEM images of vaterite-type calcium carbonate (c,d)

5.2. Powder X-ray diffractometry (pXRD)

5.2.1. Ambient & non-ambient behavior

At a first the stability of BCC-syn was investigated. The results of this part of the study were obtained from pXRD measurements. Initially, three samples were prepared and measured. Afterwards these samples were exposed to different atmospheres. One sample was stored in an exicator under dry conditions, the second sample under ambient conditions and the third one under conditions with high humidity. These samples were measured at given intervals.
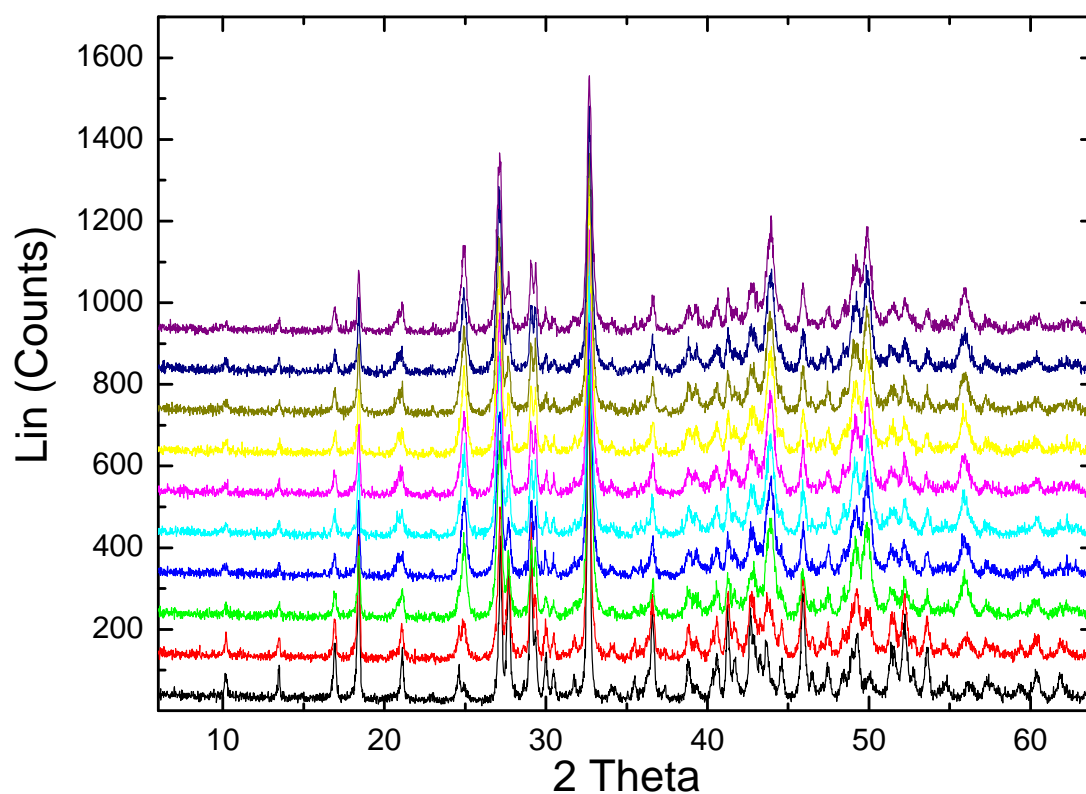
Figure 18: pXRD patterns of BCC-syn under ambient conditions (black: original BCC-syn, above: colored runs after 1/4/7/11/14/18/25/27/34 days)
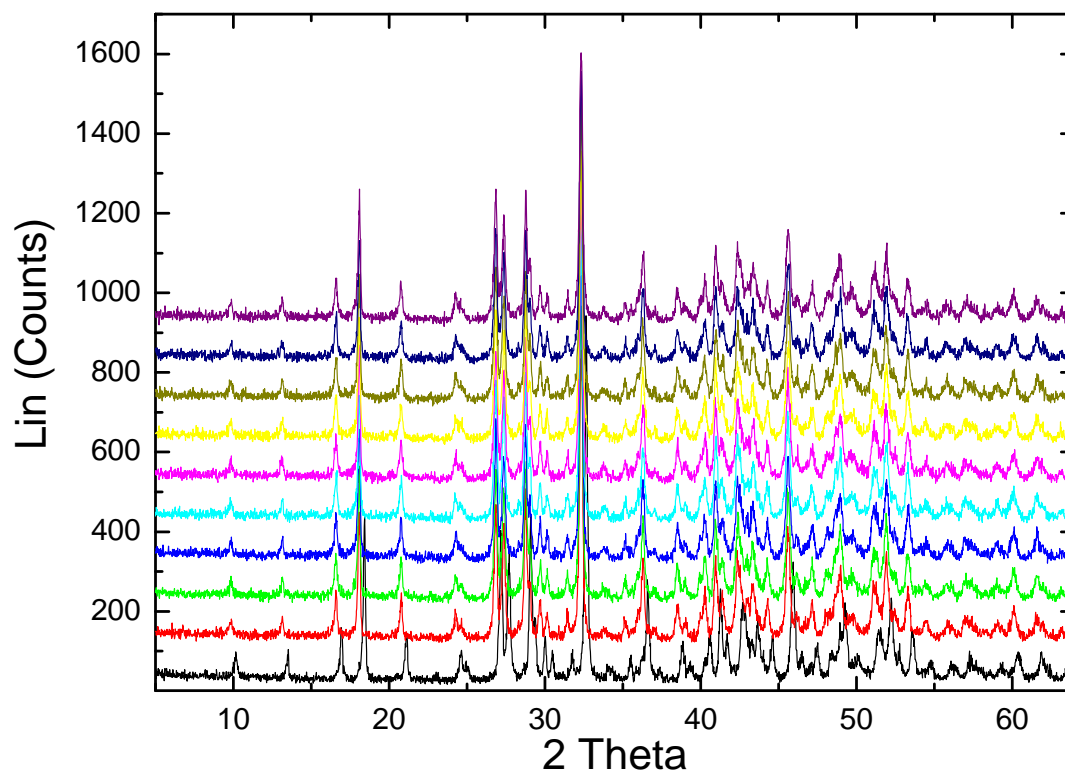
Figure 19: pXRD patterns of BCC-syn under dry conditions (black: original BCC-syn, above: colored runs after 1/4/7/11/14/18/25/27/34 days)
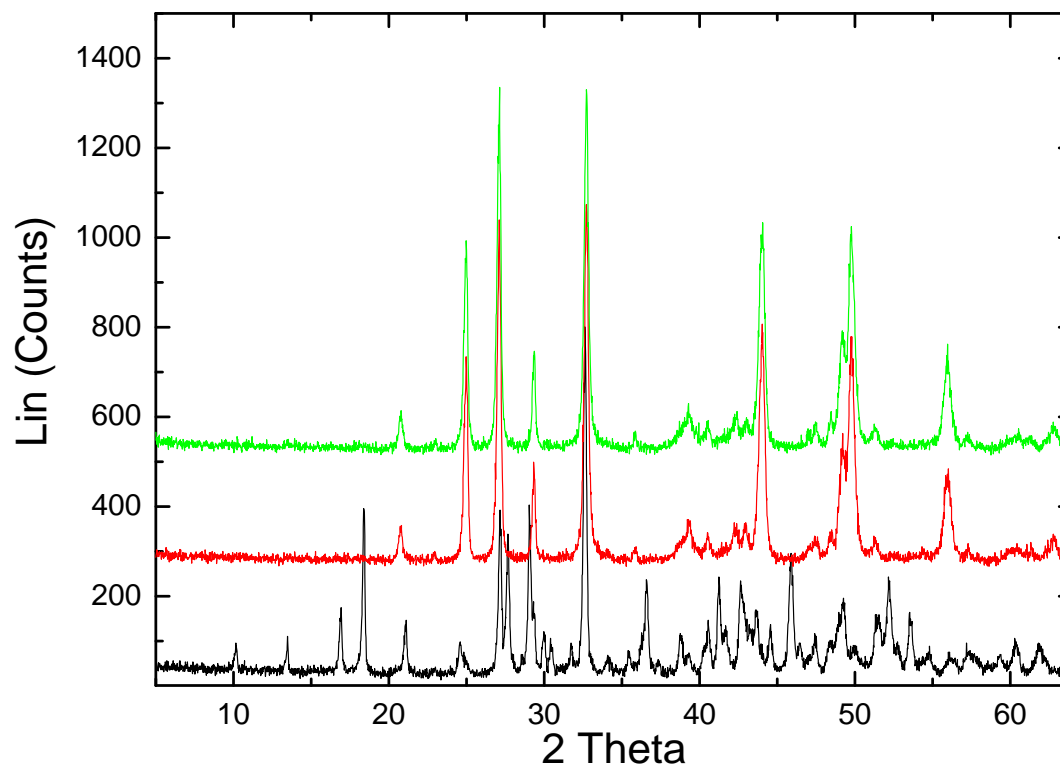

Figure 20: pXRD patterns of BCC-syn under high humidity conditions (black: original BCC-syn, above: colored runs after 1/4 days)

Figure 20 shows that under humidity saturated conditions the BCC-syn transforms rapidly into a vaterite-type calcium carbonate. However, under ambient conditions the conversion process is much slower (Figure 18), while under dry conditions the BCC is stable (Figure 19). In the latter case, even after 34 days the diffractograms shows no changes.

Additionally to the original BCC-syn, a slurry sample was provided for the study. From this suspension, BCC-slurry was prepared and compared with the BCC-syn (Figure 21). Both samples are very comparable.
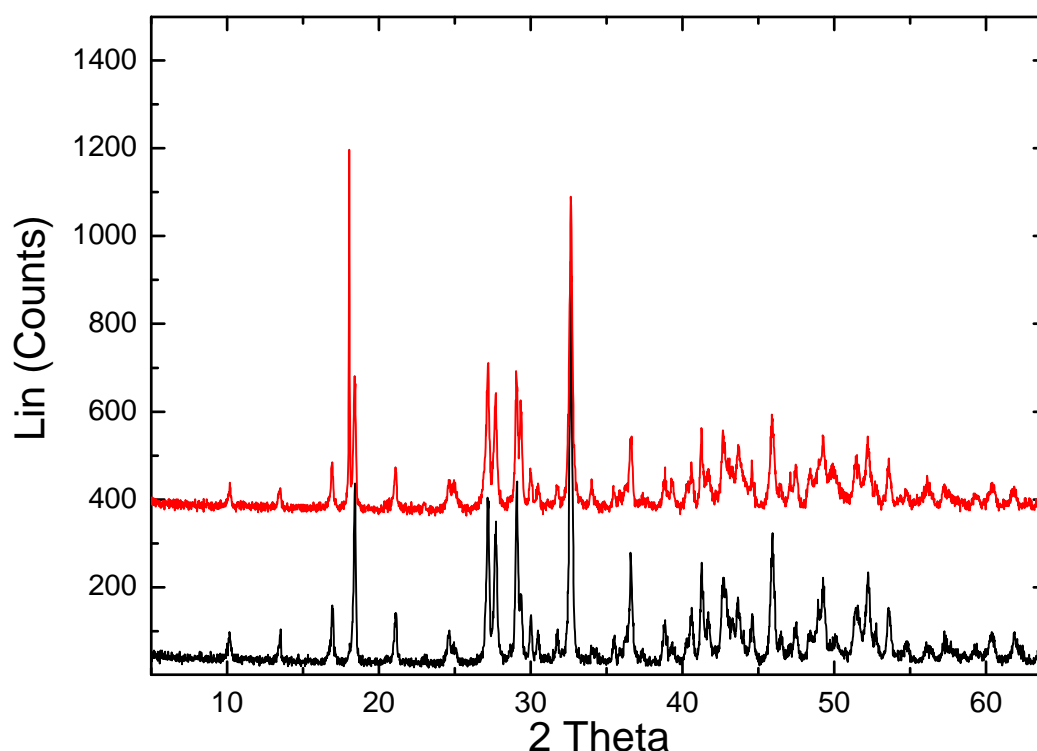

Figure 21: pXRD patterns of BCC-syn (black) and BCC-slurry (red)

After preliminary TG-measurements experiments with dehydrated BCC-syn were performed. The BCC-syn was dried for 24 hours at 225 °C. The pXRD diffractogram in Figure 22 shows fewer peaks than in the original BCC sample. In addition to BCC-syn and the dehydrated modification, the vaterite-type calcium carbonate is also shown on this plot. It is a clear outcome, that dehydrated BCC is a different phase with no similarities to any previously reported phase (Schimmel, 1970 a,b).
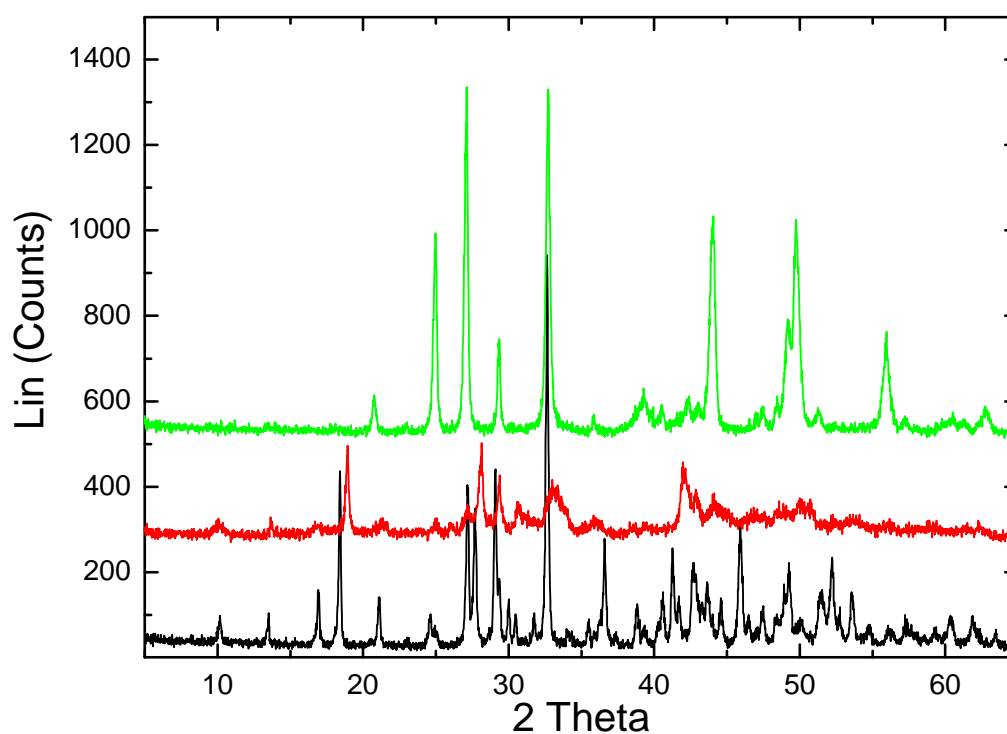
Figure 22: pXRD patterns of BCC-syn (black), BCC-dehy (red) and vaterite-type calcium carbonate (green)

The next step was to monitor the dehydrated modification, when it was stored under ambient conditions. Figure 23 plots diffractograms of the dehydrated BCC: after 0, 7 and 24 days.
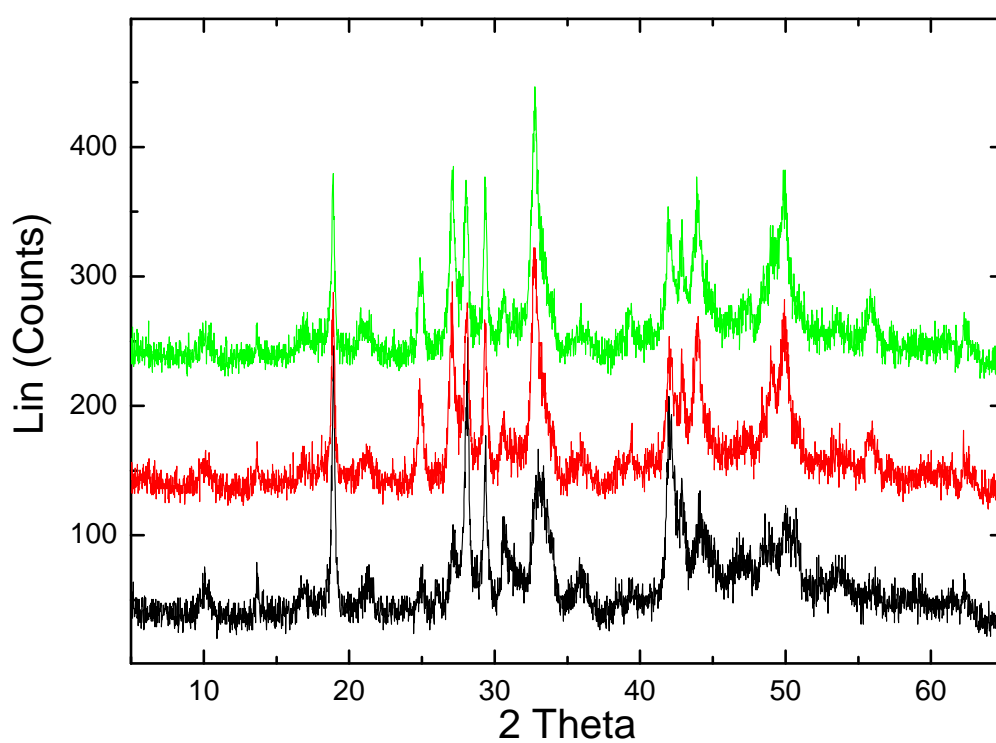

Figure 23: pXRD patterns of BCC-dehy (black: BCC-dehy, below colours: after 7/24 days)

The peak at around 25 °2θ increased, which is a strong indication that the dehydrated modification also transforms into a vaterite-type and do not transform to calcite or rehydrate to a BCC-type calcium carbonate, i.e. BCC-syn exhibit no zeolithic or clay-type behavior.
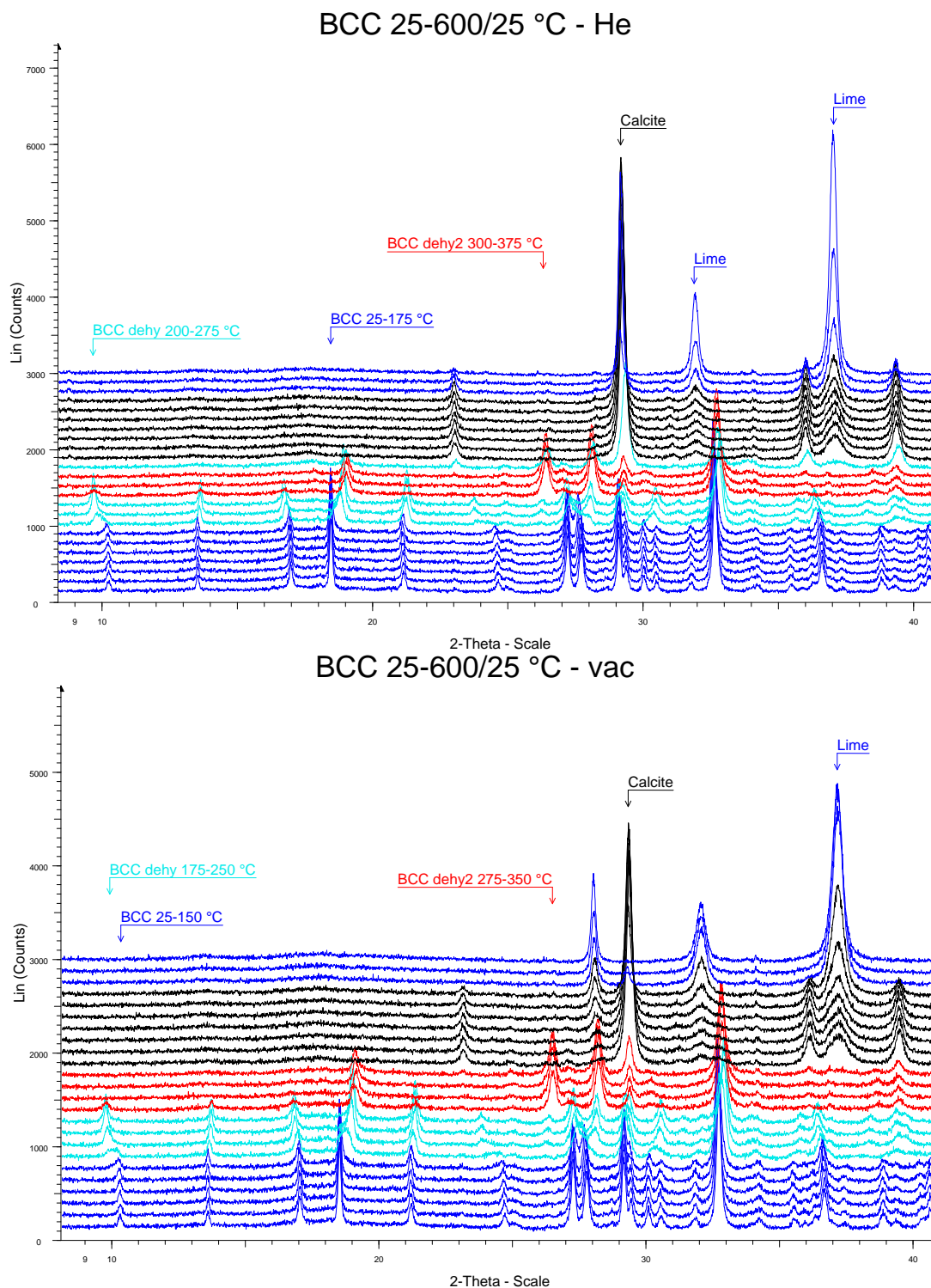

Figure 24: dT-pXRD patterns of BCC-syn under He and vacuum conditions.

Figure 24 plots the dT-pXRD patterns of BCC-syn under dry He and evacuated conditions, clearly showing BCC to be stable up to 150 °C, a continuous dehydration to a structural similar phase up to 250 °C, a hitherto unknown, structurally different dehydrated calcium carbonate phase up to 350 °C and the consecutive dehydroxylation with the formation of calcite. Consequently, the decarbonatization of calcite around 600 °C leads to the formation of lime. This thermal behavior is almost independent to the applied H_2O-free conditions during the measurements. A dehydrated form of BCC, as reported by Schimmel (1970a,b) and listed under ICDD entry 23-106 was not observed in any of the non-ambient pXRD measurements. The starting material on the other hand, resembles very well the reported powder data by Schimmel (1970a) listed under the ICDD entry 23-107.

Additional experiments were performed with the BCC-slurry. Three samples B1-3 (see section 3) were filtered and each of them was washed immediately with a different solution (B1: ethanol, B2: 1M NaOH, B3: H_2O dest.). pXRD and Raman spectroscopy (see section 5.3.) are used to investigate these treated BCC samples.
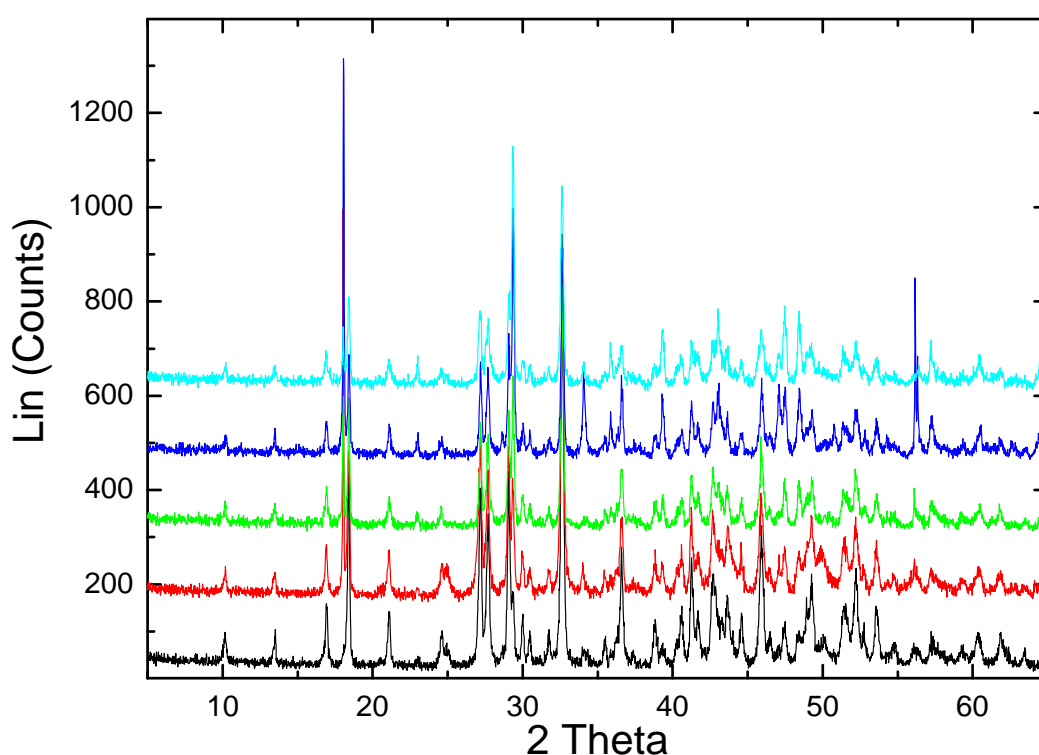

Figure 25: pXRD patterns of BCC-syn (black), BCC-slurry (red), and slurry samples B1 (green), B2 (blue) and B3 (turquoise)

It is recognizable that there are differences between the powder diffractograms. In all slurry samples a peak at around 18.3 °2θ is visible. According to the ICDD database this

peak belongs to portlandite. There are also traces of calcite in the slurry, which are also found in the different BCC's.

calcite	portlandite
°2θ	°2θ
29	18.5
36	34
47	47.5

Table 4: Significant peak positions for calcite and portlandite using Cu*K*α-radiation.
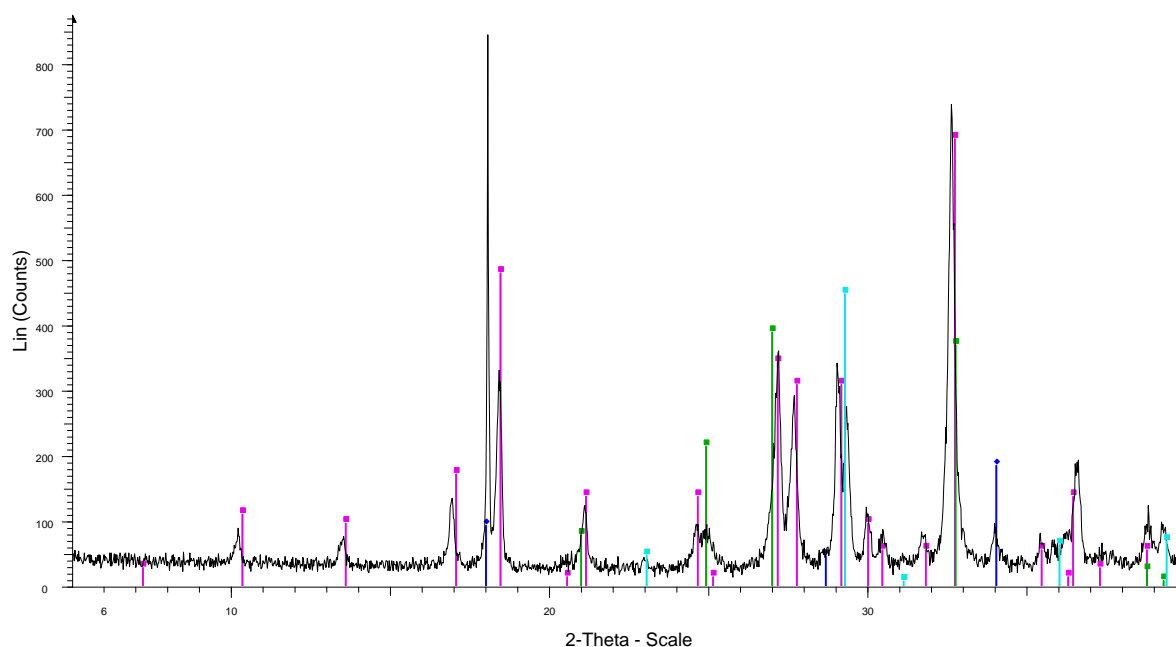

Figure 26: pXRD pattern of BCC-slurry with phase identification for calcium carbonate hydroxide hydrate (purple, ICDD: PDF 23-0107), calcite (turquoise, ICDD: PDF 86-2340), portlandite (blue, ICDD: PDF 01-1079), vaterite (green, ICDD: PDF 25-0127).

5.2.2. Structure description

The crystal structure of BCC-ori, $Ca_3(CO_3)_2(OH)_2 \cdot H_2O$, was determined by analyzing pXRD patterns. The compound is monoclinic with cell parameters $a = 8.661(1)$ Å, $b = 6.557(1)$ Å, $c = 7.078(1)$ Å and $\beta = 90.08(1)°$. The space group is Pc and the volume of this pseudo-orthorhombic unit cell is $401.97(4)$ Å³. The following Table shows all parameters of the pXRD measurements.

a [Å]	8.661(1)
b [Å]	6.557(1)
c [Å]	7.078(1)
β [°]	90.08(1)
space group	Pc
V [Å³]	401.97(4)
Z	2
ρ_{calc} [g/cm³] (without H-atoms)	2.38
range of data collection [°]	$7.0 < 2\theta < 67.5$
Step size [°]	0.008
Time/step [s]	0.2
divergence slit width [mm]	6.00
r_wp [%]	9.6
Bruker D8 X-ray diffractometer with a position sensitive device (PSD) LynxEye detector system. To determine the modal mineral composition semi quantitative Rietveld refinement calculations of the analyzed pXRD patterns were done by using the program TOPAS.	

Table 5: pXRD data-collection and structure refinements of BCC-ori

The data which are used for the structure determination powder diffraction are shown in Figure 27. Approximately 94 % of the investigated powder is BCC-ori. Additionally, there are amounts of calcite and traces of vaterite and portlandite. The powder pattern also shows that there are strong reflections up to 55 °2θ. Accordingly, the structure is a model, which cannot be compared with a single crystal determination. The result after the structure refinement gave an r_wp value of 9.6 %. For the refinement several anti-bump terms were defined, which prevent that those atoms do not come too close to each other. These are listed in Table 6.

Ca*-O* [Å]	2.1
C*-O* [Å]	1.2
O*-O* [Å]	2.1

Table 6: Anti-bump terms for the structure refinement (* for all atoms of O and C)

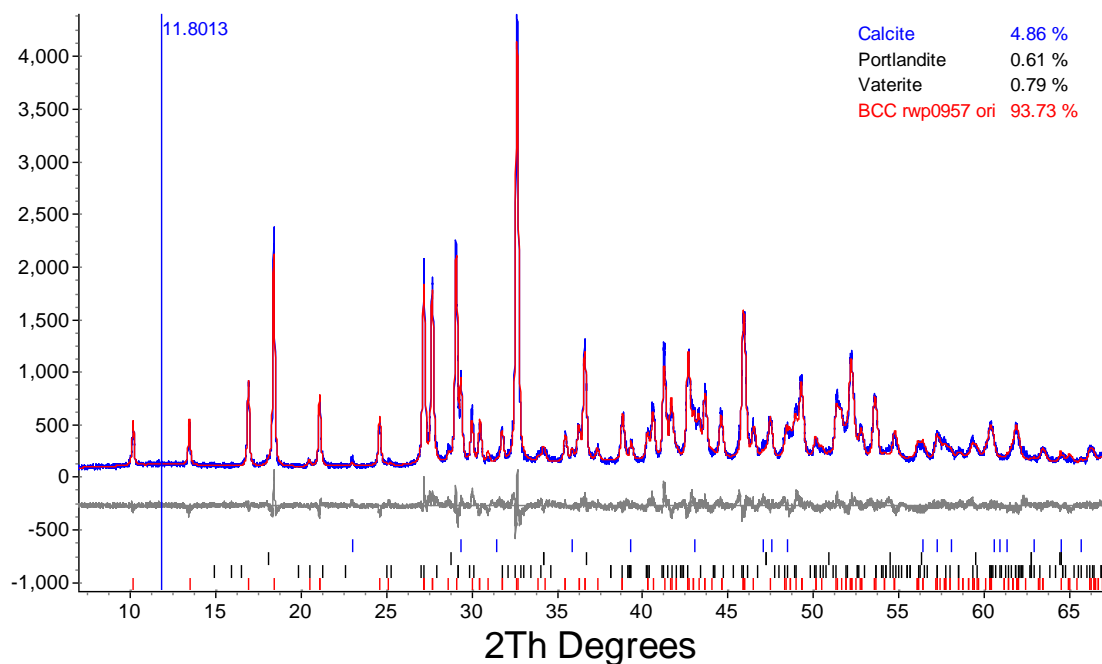**Figure 27:** Rietveld plot of BCC-ori.

Structure model:

The chemical formula of BCC is $Ca_3(CO_3)_2(OH)_2 \cdot H_2O$. So the unit cell contains 28 atoms. Because of the formula unit of two, there are 14 atoms to describe. All atoms are located at general positions, with a multiplicity of 2 [(1) x,y,z; (2) $x,-y,z+0.5$].

Atoms*	x	y	z
Ca1	0.106	0.823	0.744
Ca2	0.816	0.547	0.448
Ca3	0.557	0.825	0.752
C1	0.800	0.975	0.934
C2	0.301	0.200	0.575
O1	0.800	0.790	0.898
O2	0.346	0.272	0.037
O3	0.941	0.941	0.902
O4	0.980	0.980	0.505
O5	0.365	0.365	0.708
O6	0.069	0.687	0.916
O7	0.619	0.614	0.501
O8	0.388	0.388	0.887
O9	0.149	0.149	0.857

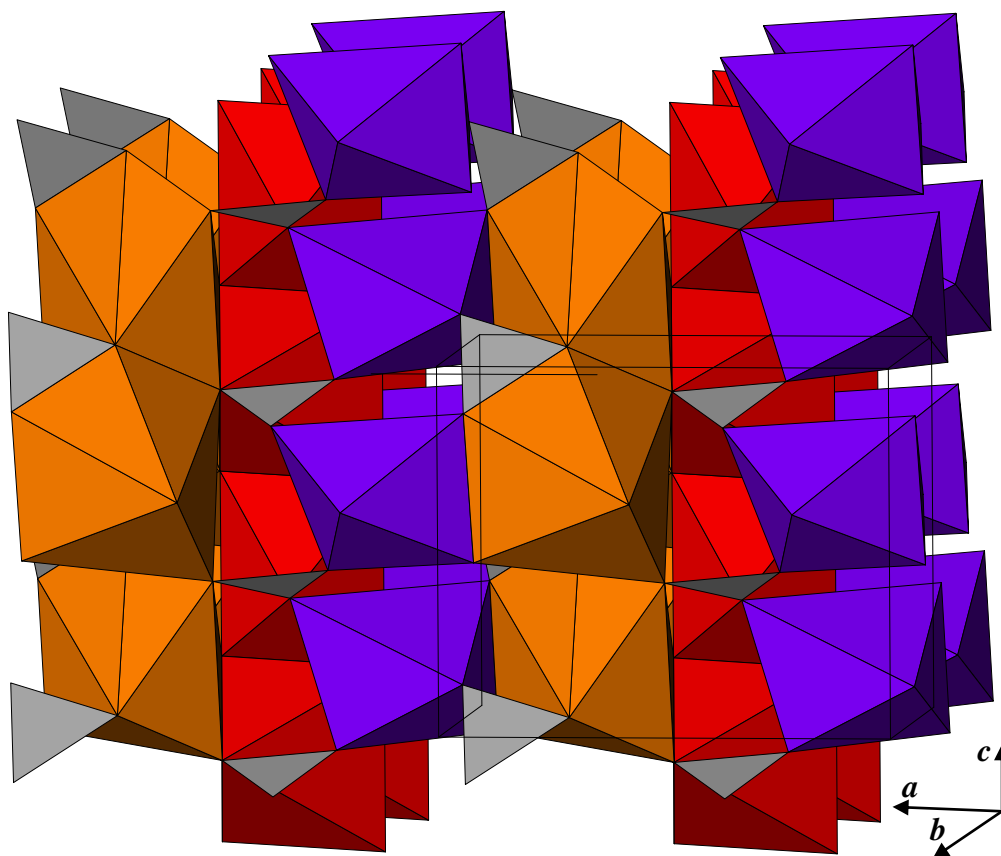**Table 7:** Atom positions of the structure model. (*all coordinates fixed)

Figure 28: Structure model of BCC-ori (orange: Ca1[7], red: Ca2[6], purple: Ca3[6], grey: C1[3],C2[3])

This structure model contains three nonequivalent Ca-O polyhedron, which are among themselves edge-linked. Basically, the C-O triangles are corner connected to the Ca-O polyhedra, except for the Ca1-C2 connection. This is due to the seven-coordinated calcium atom. The other two six-coordinated calcium atoms are corner connected to the carbon triangles. Along the *c*-axis there is a infinite chain of edge connected Ca2-O polyhedra. This is a characteristic structure motiv, which also can be seen in the structure of the related compound hydromagnesite. Due to the fact that these findings are based on powder data, it is impossible to locate any hydrogen atoms. The possible oxygen atoms, which are hydrogen-bonded can only be determined with the bond-valence parameters after Brese & O'Keeffe (1991). This part is discussed later.

The following Table 8a,b lists the interatomic bond lengths, bond angles and distortion parameters (Fleet, 1976) for BCC-ori.

Bond lengths [Å] *			
Ca1-O9	2.330	Ca3-O6	2.196
Ca1-O4	2.425	Ca3-O7	2.237
Ca1-O3	2.468	Ca3-O5	2.261
Ca1-O9	2.624	Ca3-O1	2.353
Ca1-O2	2.628	Ca3-O8	2.424
Ca1-O5	2.751	Ca3-O2	2.456
Ca1-O3	2.796	<Ca3[6]-O>	2.321
<Ca1[7]-O>	2.575	C1-O1	1.240
Ca2-O4	2.192	C1-O1	1.313
Ca2-O1	2.241	C1-O1	1.478
Ca2-O4	2.387	<C1[3]-O>	1.343
Ca2-O7	2.431	C2-O1	1.261
Ca2-O7	2.519	C2-O1	1.262
Ca2-O3	2.574	C2-O1	1.387
<Ca2[6]-O>	2.391	<C2[3]-O>	1.304

Distortion parameters			
Ca1	QE	λ	1.0039
	BAV	σ^2	-
Ca2	QE	λ	0.8650
	BAV	σ^2	176.4
Ca3	QE	λ	0.8141
	BAV	σ^2	304.3

Table 8a: Bond lengths in [Å] (*fixed) and distortion parameters (after Fleet, 1976) of BCC-ori

Bond angles [°] *						
Ca1[7]	O9:1	O4:1	O3:0	O9:0	O2:1	O5:0
O9:1	-	-	-	-	-	-
O4:1	146.93	-	-	-	-	-
O3:0	65.41	82.00	-	-	-	-
O9:0	107.66	102.79	147.41	-	-	-
O2:1	81.83	95.63	93.96	117.22	-	-
O5:0	108.71	99.49	158.29	53.70	64.33	-
O3:1	74.81	112.92	91.08	57.10	151.44	107.90

Ca2[6]	O4:0	O1:1	O4:1	O7:0	O7:1
O4:0	-	-	-	-	-
O1:1	78.45	-	-	-	-
O4:1	101.17	91.31	-	-	-
O7:0	165.20	86.88	80.91	-	-
O7:1	82.84	73.69	163.52	91.26	-
O3:0	83.27	158.16	80.55	111.48	115.90

Ca3[6]	O6:0	O7:0	O5:0	O1:0	O8:1
O6:0	-	-	-	-	-
O7:0	87.91	-	-	-	-
O5:0	161.40	88.49	-	-	-
O1:0	85.65	77.15	111.28	-	-
O8:1	88.07	148.54	85.52	133.55	-
O2:1	86.71	79.11	74.70	155.28	69.52

C1[3]	O1:0	O6:1
O1:0	-	-
O6:1	127.93	-
O3:1	124.98	104.71

C2[3]	O5:1	O8:1
O5:1	-	-
O8:1	117.05	-
O9:1	133.09	108.95

Table 8b: Bond angles in [°] (*fixed) of BCC-ori

Hydrogen-atoms and bond-valence parameters:

As previously mentioned the hydrogen atom positions cannot be located because of the limits of pXRD data. The only option is to find the possible oxygen atoms, which have bond to a hydrogen atom. For this purpose the bond-valence parameters after Brese & O'Keeffe (1991) were calculated in an excel-sheet.

	Ca1	Ca2	Ca3	C1	C2	Σv
O1		0.48	0.35	1.50		2.33
O2	0.17	0.28				0.45
O3	0.26 0.11	0.20		0.79		1.36
O4	0.29	0.54 0.32				1.15
O5	0.12		0.45		1.42	1.99
O6			0.54	1.23		1.77
O7		0.29 0.23	0.48			1.00
O8			0.29		1.41	1.70
O9	0.38 0.17				1.01	1.56
Σv	1.50	2.34	2.11	3.52	3.84	

Table 9: Bond-valence parameters (after Brese & O'Keeffe) of BCC-ori

According to the values in Table 9, there are three oxygen atoms (O2,4,7) with a bond-valence parameter much smaller than two. From that it can be concluded that these atoms have a further bond to a hydrogen atom. O2 have a bond strength of 0.434, which is a typically value for a water molecule. Possible OH-groups are the oxygen atoms 4 and 7 with a value of 1.156 and 0.993. In Figure 29 these oxygen atoms are shown in the structure model. It can be seen that the Ca1 atom is far away of the set value 2, which lead back to the pXRD data. Generally different deviations of all atoms are obtained, which still let some open points for discussion.
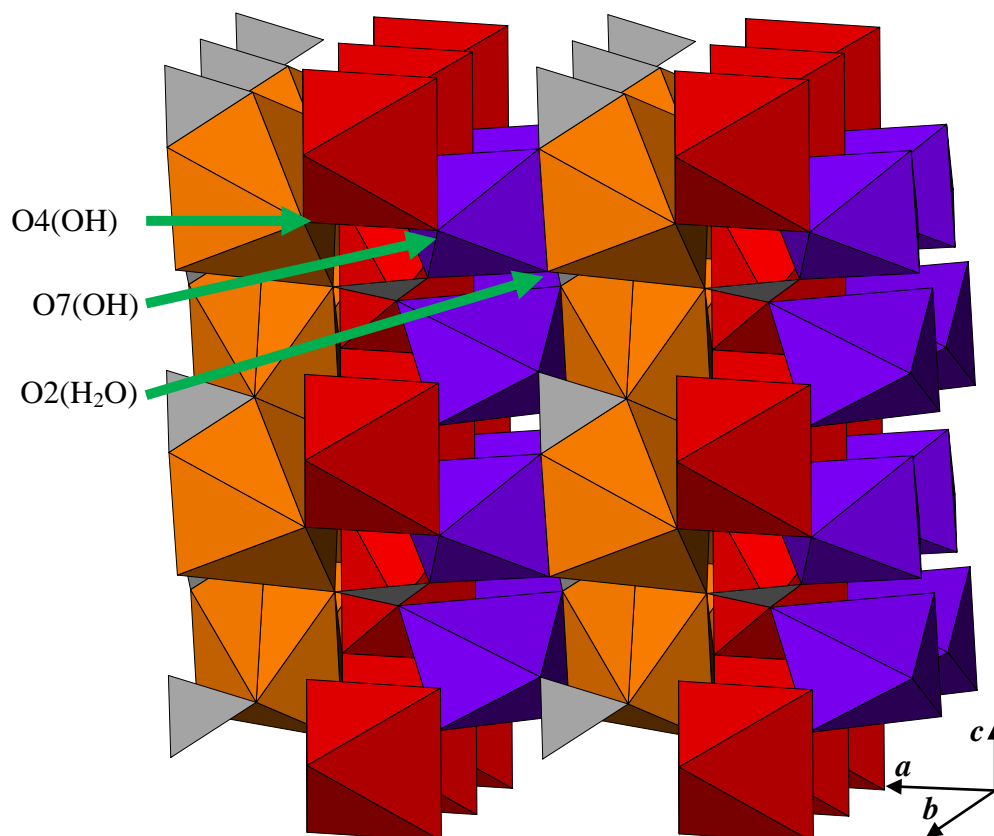
Figure 29: Structure model of BCC-ori with the possible oxygen positions for H_2O and OH-groups.

Comparison with other structures:

Of course the structure model of BCC-ori should have similarities with the starting material, portlandite, as well as the conversion product, vaterite. The following Figures 30-32 show the structures in comparison. The portlandite structure consists of edge-linked calcium octahedra. This can be seen also in the BCC structure model. Hereby the similarities are a coordination number of 6 and the edge-linked polyhedra. Other resemblances are obtained between BCC-ori and the conversion product, vaterite. The common features are the higher coordinated calcium atom and the edge-connection of one carbon polyhedron. Further orthorhombic vaterite exhibits chains along the *c*-axis with corner-connected calcium polyhedra.
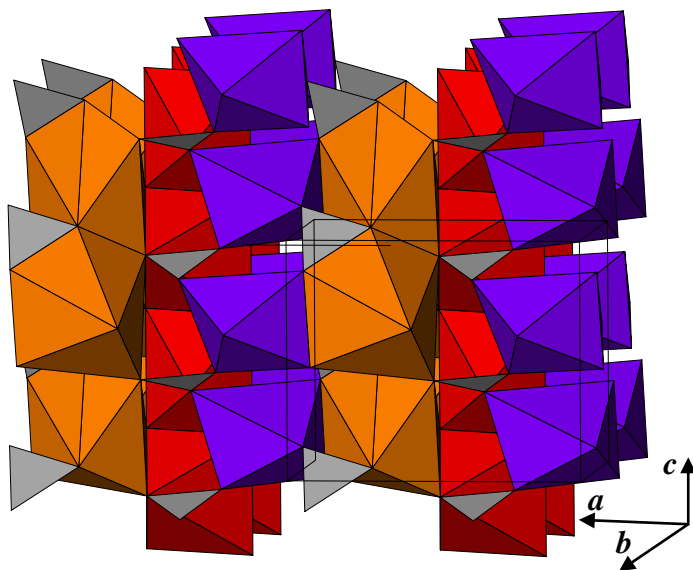
Figure 30: Structure model of BCC-ori (orange: Ca1[7], red: Ca2[6], purple: Ca3[6], grey: C1[3],C2[3])
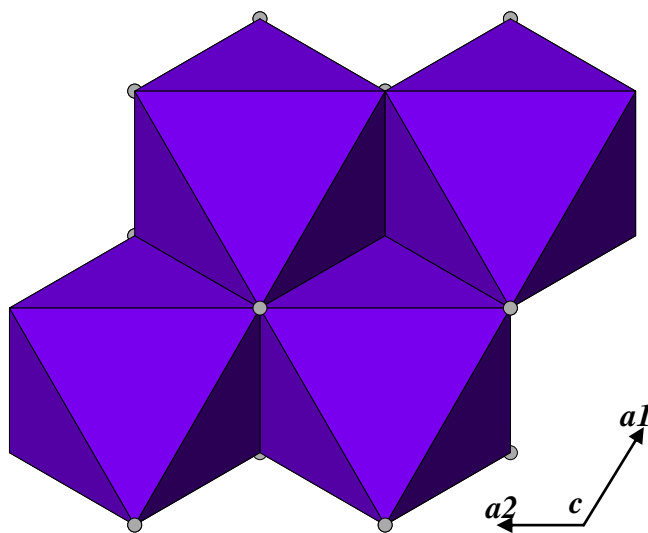
Figure 31: Crystal structure of portlandite, $Ca(OH)_2$, after Petch (1961)
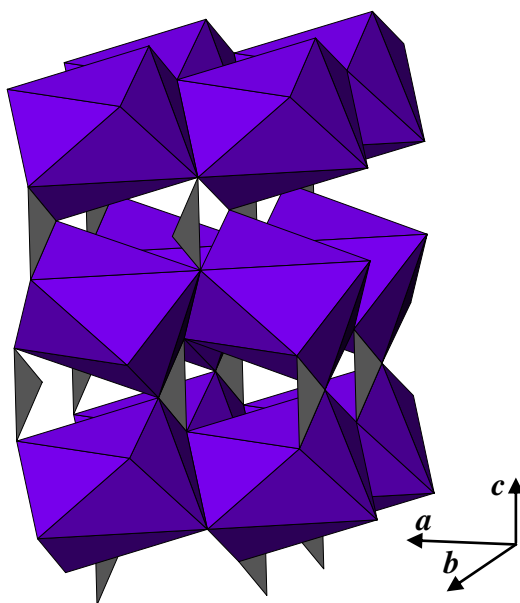
Figure 32: Crystal structure of orthorhombic vaterite, $CaCO_3$, after Meyer (1960)

Such basic BCC's are known approximately since the 1970's (Schimmel, 1970). Even longer the group of the basic magnesium carbonates is known. Pietsch (1939) described two minerals and their synthesis. Meanwhile there are nine known minerals in the hydromagnesite-artinite group. For the calcium analogues there are no minerals reported. So the BCC structure model was compared with the crystal structure of hydromagnesite. The chemical formula of this mineral is $Mg_5(CO_3)_4(OH)_2 \cdot 4H_2O$ and have a monoclinic unit cell with a volume of 688.8 Å³. (Akao et al., 1977)
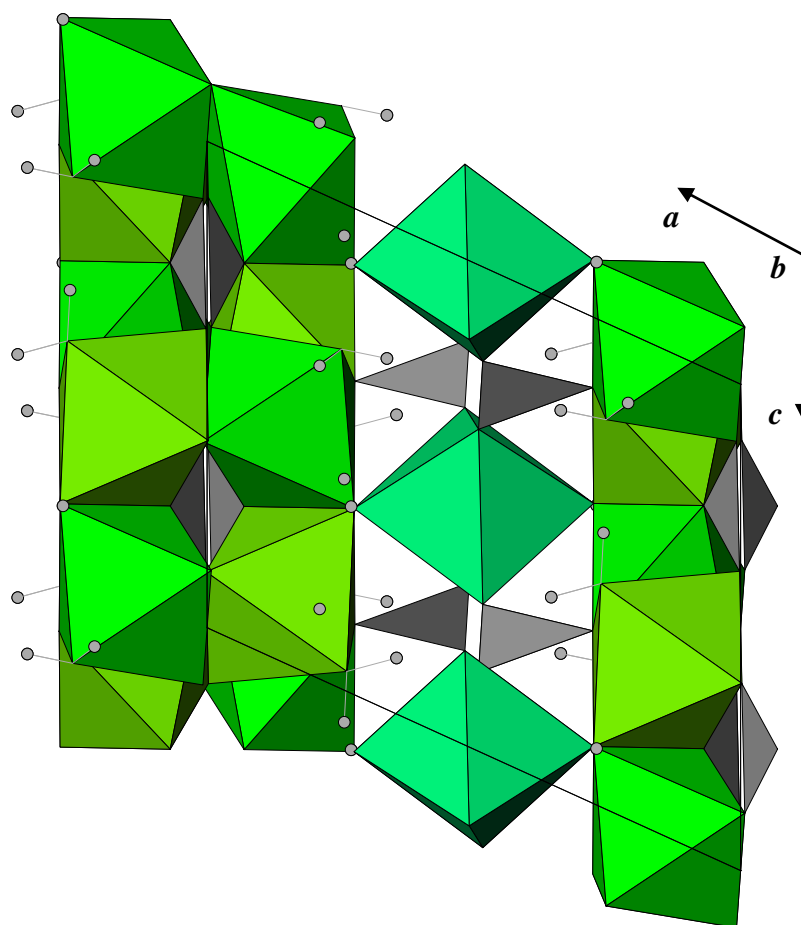
Figure 33: Crystal structure of hydromagnesite , after Akao et al. (1977)

As in the structure of BCC-ori there are also chains of edge-linked calcium polyhedra along the *c*-axis. The chains are connected with a third magnesium polyhedron along the *a*-axis. This is a very similar feature to the Ca1-polyhedron in the BCC model. It is worth to point out that the structure contains the same count of atoms as in the BCC model: 3 magnesium, 2 carbon and 9 oxygen atoms.

5.3. Spectroscopy

5.3.1. Infrared spectroscopy (IR)

Samples were also investigated with infrared and Raman spectroscopy (Table 3). With the help of these methods, qualitative results can be obtained due to the characteristic molecular and lattice vibrations. Some vibrations are only IR or Raman active, therefore these methods are a mutual complement to each other.
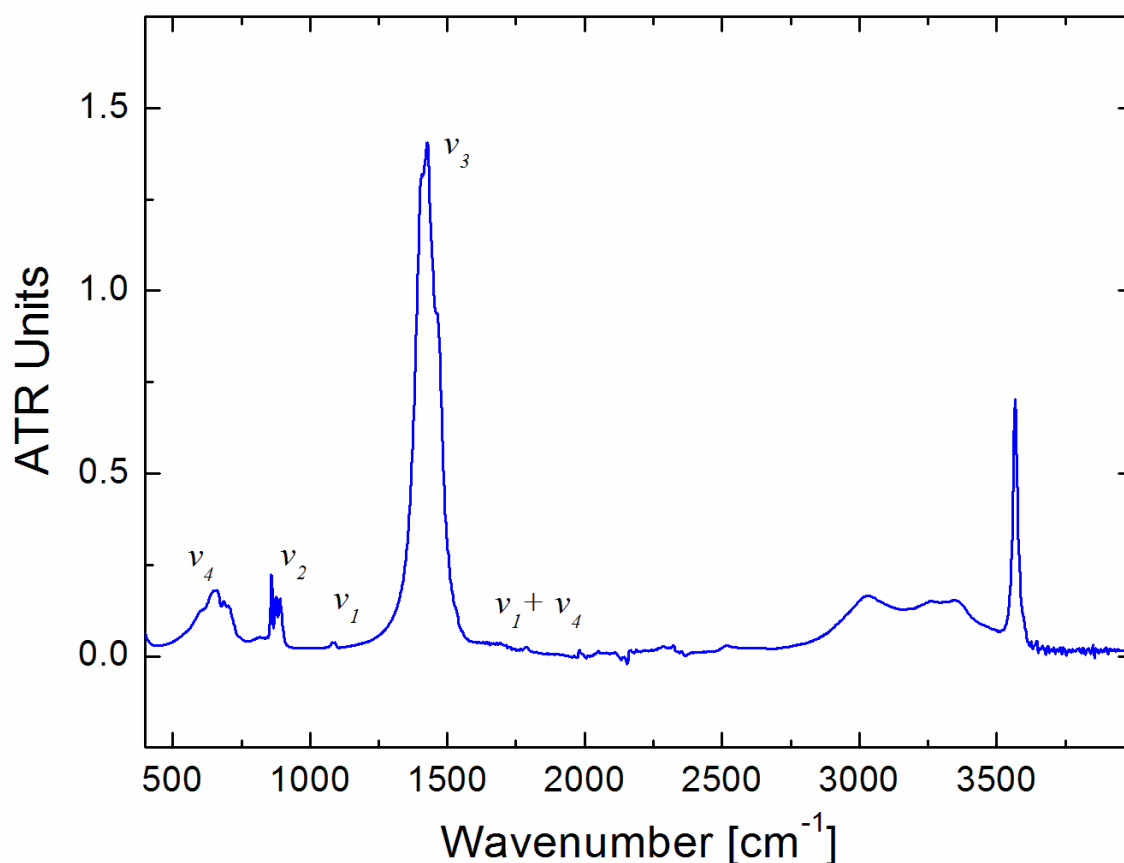
Figure 34: IR spectrum of BCC-syn, recorded with ATR unit.

In the spectrum in Figure 34 one can observe the strong characteristic carbonate vibrations at approximately 1500 cm^{-1}. v_1 to v_4 are all carbonate vibrations in a range of 1800 to 500 cm^{-1}. v_3 is the antisymmetric stretching vibration, v_2 and v_4 the symmetric and antisymmetric bending vibration, respectively. There is also a signal around 1080 cm^{-1}, which is the not IR active symmetric stretching vibration. In addition a combination vibration of v_1 to v_4 becomes visible. At 3600 cm^{-1} the O-H stretching vibration is clearly recognizable, but the O-H bending vibration at 1600 cm^{-1} is missing. In comparison to this record, another measurement was performed with a KBr-pellet, which is shown in Figure 35. The only difference between these two data sets is the red-shift in the ATR spectrum

and the CO_2 artefact at 2300 cm^{-1} in the KBr spectrum, which arises from the ambient conditions.
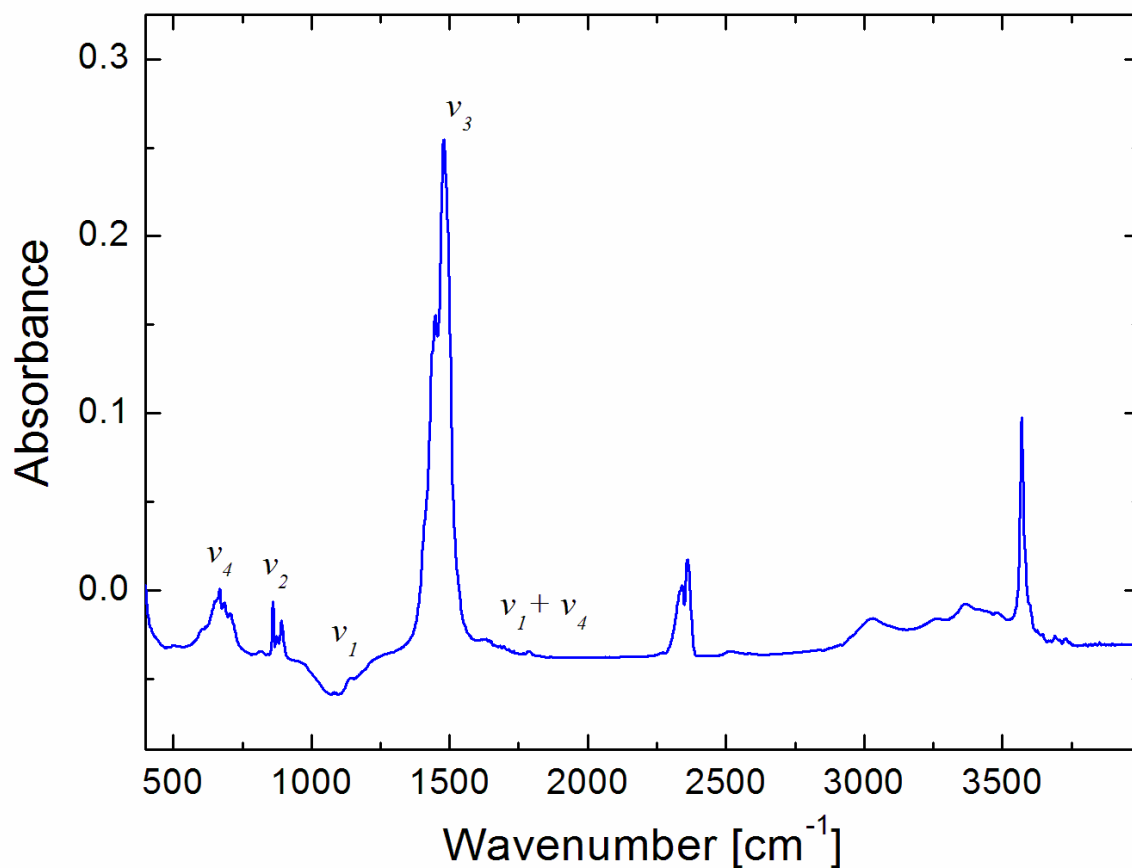
Figure 35: IR spectrum of BCC-syn, prepared with KBr-pellet.

Further infrared spectra were recorded for the BCC-slurry, BCC-dehy and vaterite-type calcium carbonate (Figure 36,37,38). In the spectrum of the dehydrated modification, the O-H stretching vibration almost disappears. Moreover the peak from the CO_3 antisymmetric stretching vibration split up, possibly due to stress or surface effects (Figure 37). The spectrum of vaterite-type calcium carbonate exhibits carbonate peaks and no O-H stretching vibrations at 3600 cm^{-1}. The Peak at around 2900 cm^{-1} is an artifact from the pXRD sample holder (Figure 38).
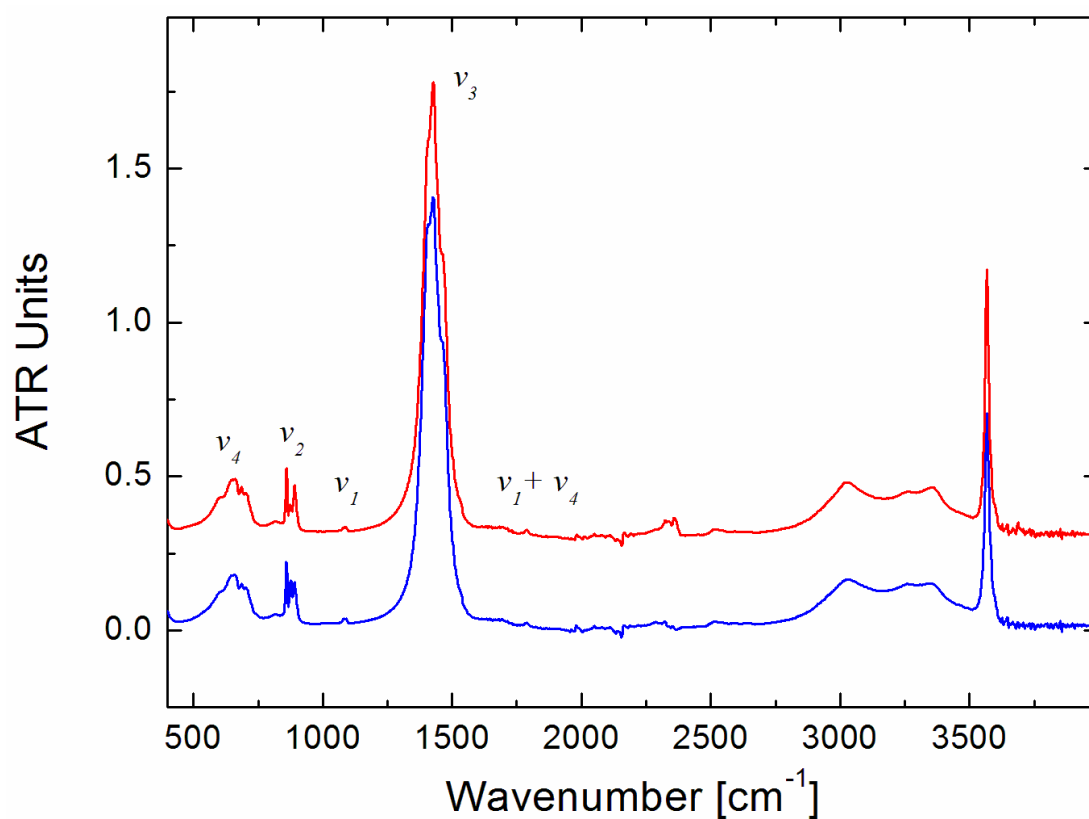
Figure 36: IR spectra of BCC-syn (blue) and BCC-slurry (red)
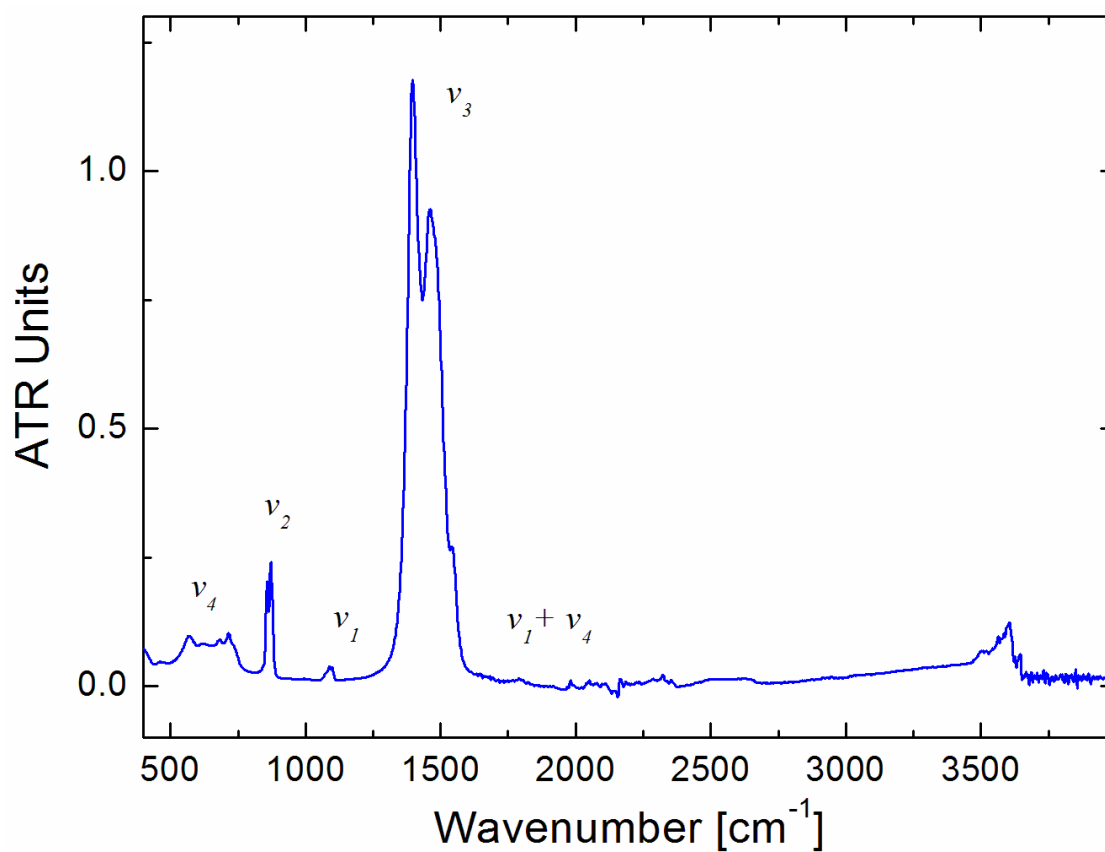
Figure 37: IR spectrum of BCC-dehy
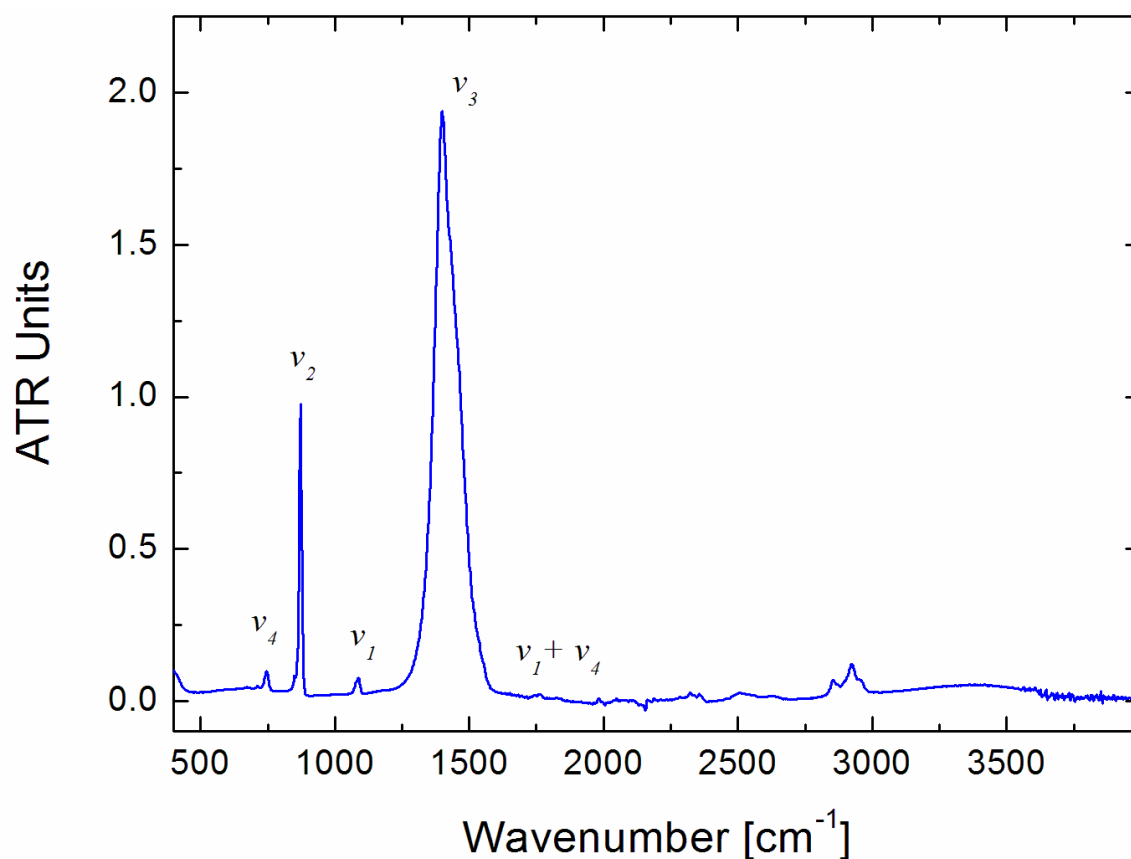
Figure 38: IR spectrum of vaterite-type calcium carbonate

Vibration	$\tilde{v}[cm^{-1}]$
v_4 antisymmetric bending vibration (Fig.34-38)	685, 653, 609
v_2 symmetric bending vibration (Fig.34-38)	890, 876, 858
v_1 symmetric stretching vibration (Fig.34-38)	1078
v_3 antisymmetric stretching vibration (Fig.34-38)	1424
$v_1 + v_4$ combination vibration (Fig.34-38)	1785
O-H stretching vibration (Fig.34-37)	3567
H_2O bending vibration	~1600
CO_2 vibrations (artefact) (Fig.35)	2356, 2341
C-H vibrations (artefact) (Fig.38)	2951, 2920, 2853

Table 10: IR-vibrations and their related peak positions for BCC compounds.

5.3.2. Raman spectroscopy

Complementary to infrared spectroscopy, investigations were performed with Raman spectroscopy. The measurements were recorded with a 633 nm laser excitation in a range of 4000 to 60 cm^{-1}.
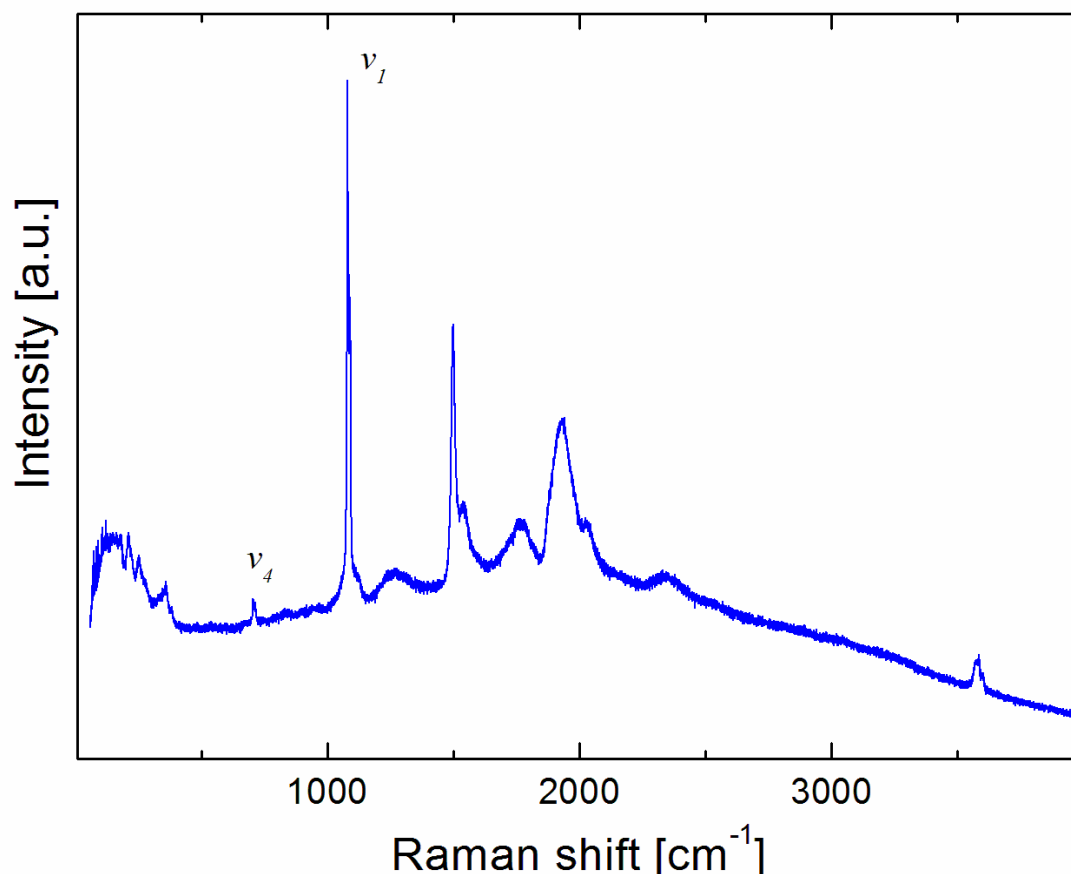
Figure 39: Raman spectrum of BCC-syn

In literature there are no Raman data of this calcium carbonate hydroxide hydrate given, so it is not stringent to assign peaks and interpret the spectra. In the spectrum of the BCC-syn are two characteristic vibrations of the carbonate group: the symmetric stretching vibration v_1 at 1080 cm^{-1} and the antisymmetric bending vibration v_4 at 710 cm^{-1}. The symmetric bending vibration is missing, because it is not Raman active. At 3575 cm^{-1} the O-H stretching vibration is clearly visible and it is in agreement with the IR spectra. BCC-dehy shows a related spectrum to BCC-syn (Figure 40). Raman spectra of vaterite-type calcium carbonate (Figure 41) are known from literature, so the recorded spectrum can be well compared to these references. The characteristic peaks at ~1100, 750, 310 to 280, and 114 to 106 cm^{-1} are corresponding to these data (Caracas et al., 2011).
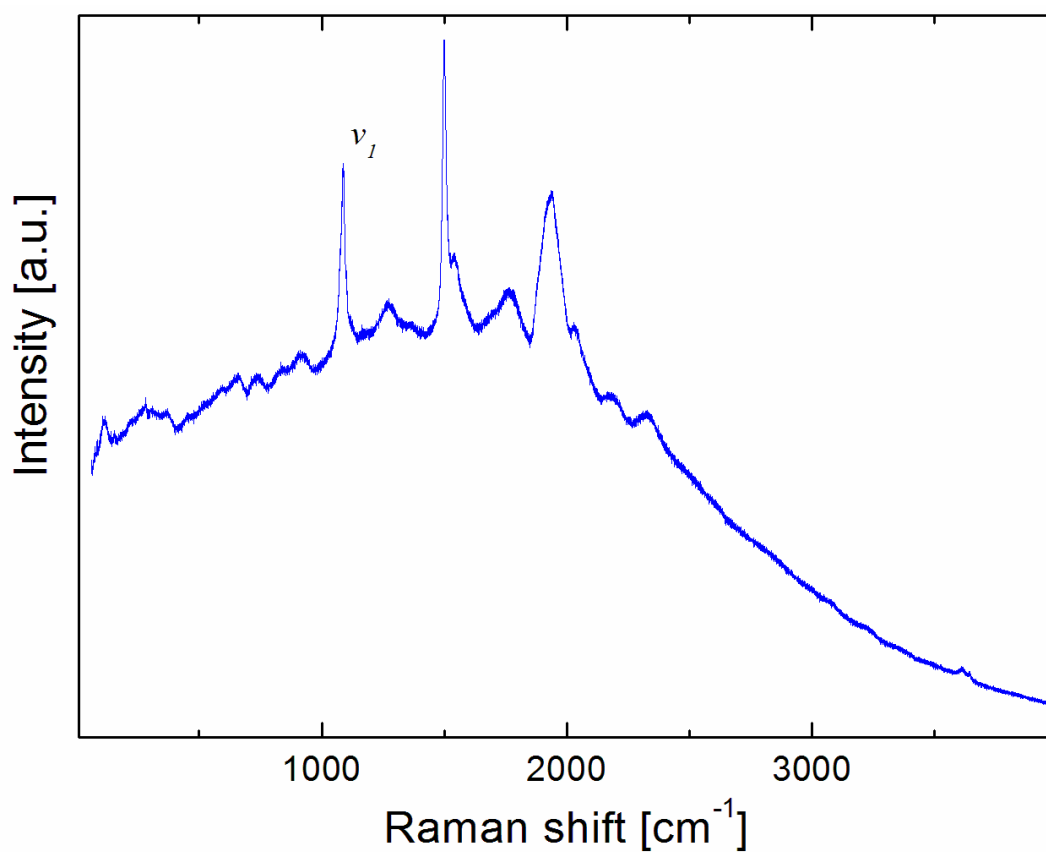
Figure 40: Raman spectrum of BCC-dehy
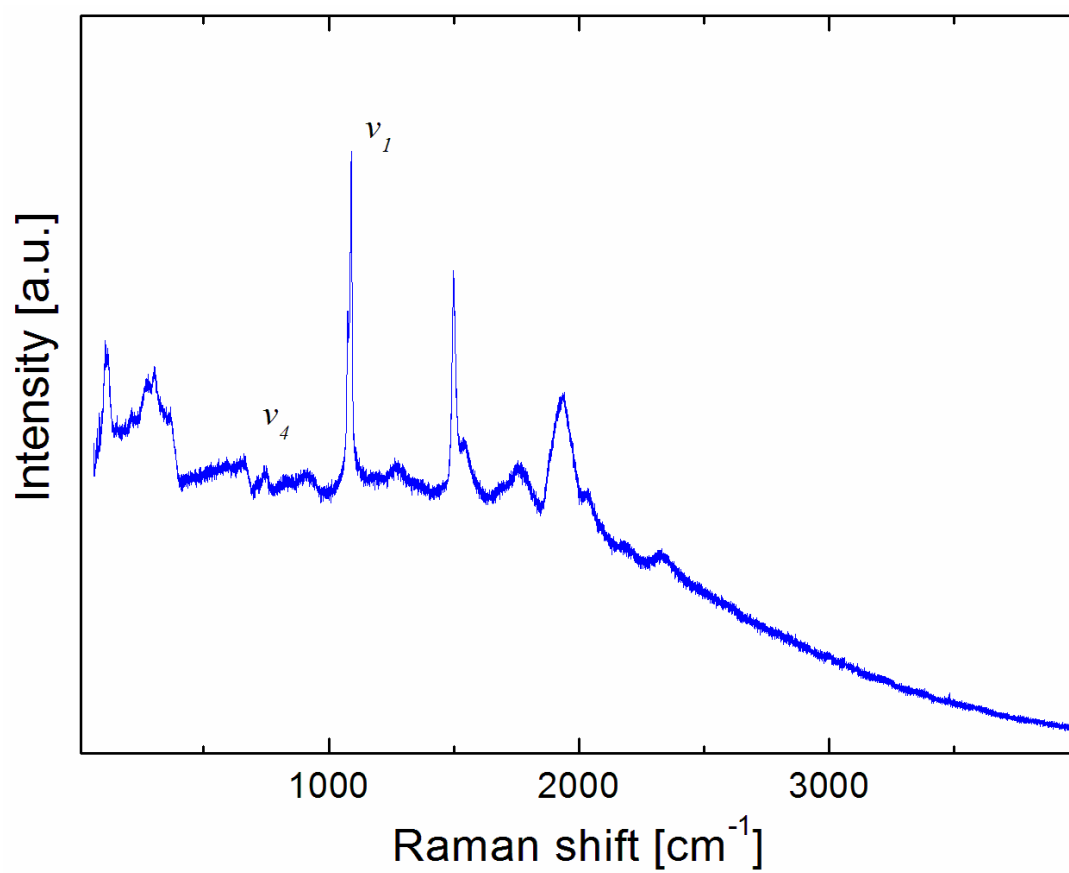
Figure 41: Raman spectrum of vaterite-type calcium carbonate

The peaks of the O-H stretching vibration in the spectrum of BCC-dehy are blue shifted and have a better split, which can be a reference to regeneration or crystallization caused by the increase of temperature.
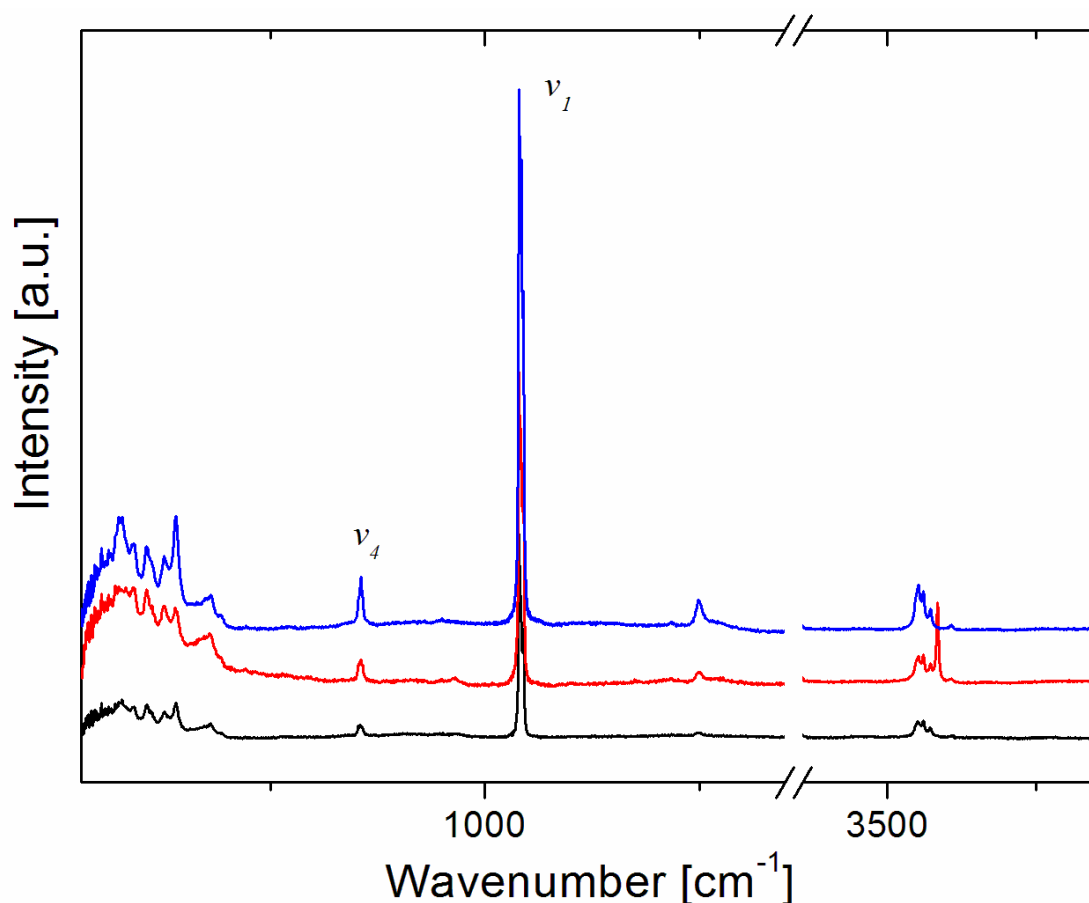
Figure 42: Raman spectra of the BCC-slurry samples B1 (black), B2 (red) and B3 (blue)

With Raman spectroscopy the products can be confirmed. Other artifacts were also determined with this method. The three spectra look like the existing data, except small differences. The vibrations of the carbonate group can be seen at 710 cm^{-1} and 1080 cm^{-1} as well as the O-H stretching vibration at 3600 cm^{-1}. The internal structure of the peak at 1080 cm^{-1} and the peak group at 3600 cm^{-1} is slightly different.

A further experiment with a heating stage was performed. For this the sample was heated up to 300 °C. There are no anomalies, except the weak intensity and the larger peak width at higher temperatures. These effects are shown in the following Figures 43 and 44.
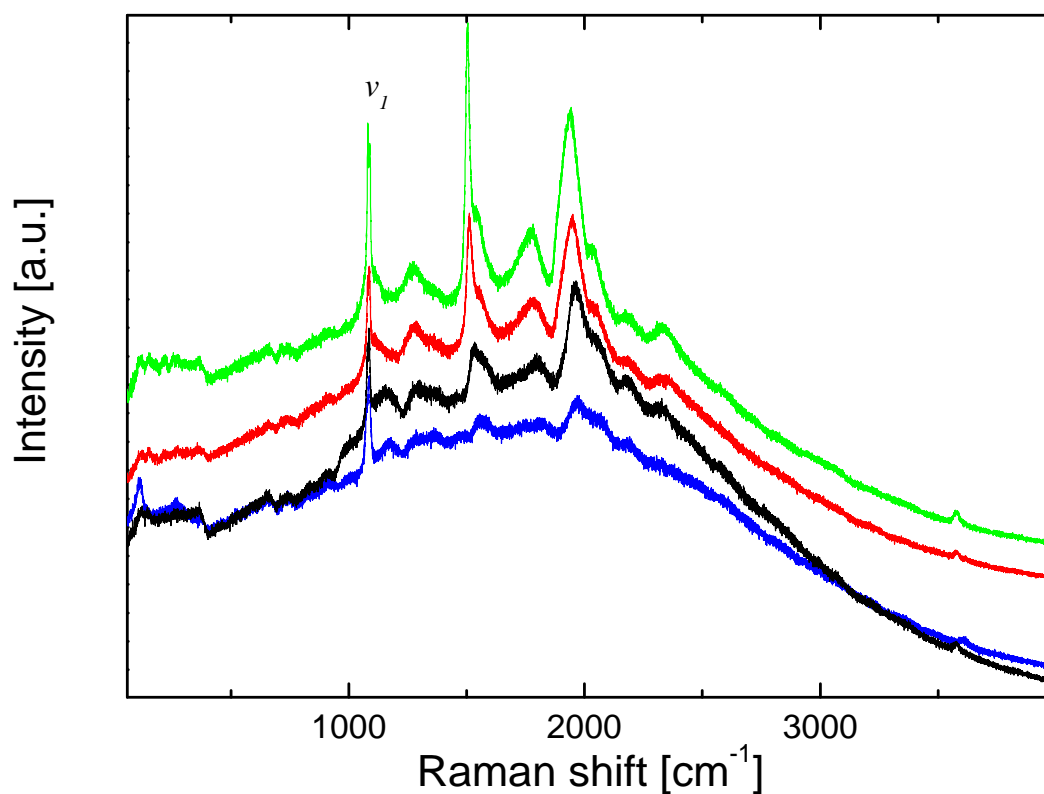
Figure 43: Raman spectrum of BCC-syn during the heating process. (green: 50 °C, red: 100 °C, black: 200 °C, blue: 300 °C), Range: 60-4000 cm^{-1}
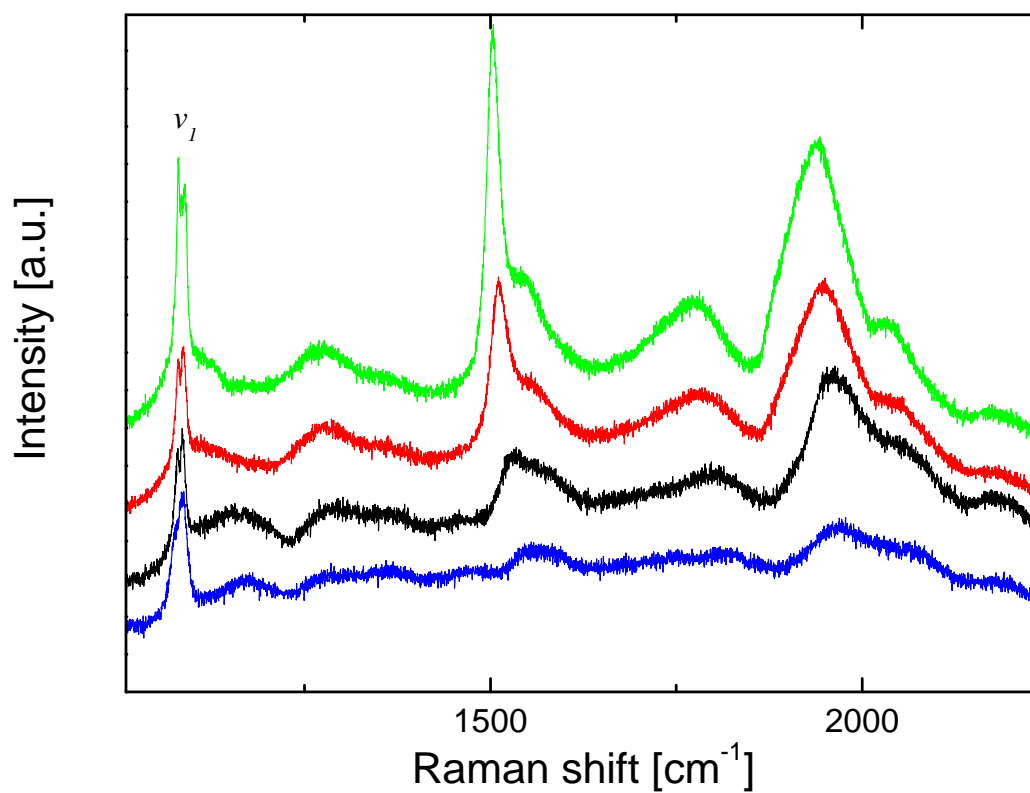
Figure 44: Raman spectrum of BCC-syn during the heating process. (green: 50 °C, red: 100 °C, black: 200 °C, blue: 300 °C), Range: 1000-2250 cm^{-1}

5.4. Thermal analyses

5.4.1. Thermogravimetry (TG)

The thermogravimetric analysis shows three weight losses in a temperature range of 25 to 900 °C (Figure 45). The two endothermic processes in a range of 150 to 500 °C can be assigned to the loss of two different, chemical bonded water contents (-6.7 wt% and -5.6 wt%). The third significant weight loss of approximately -31 wt% corresponds to the release of CO_2.
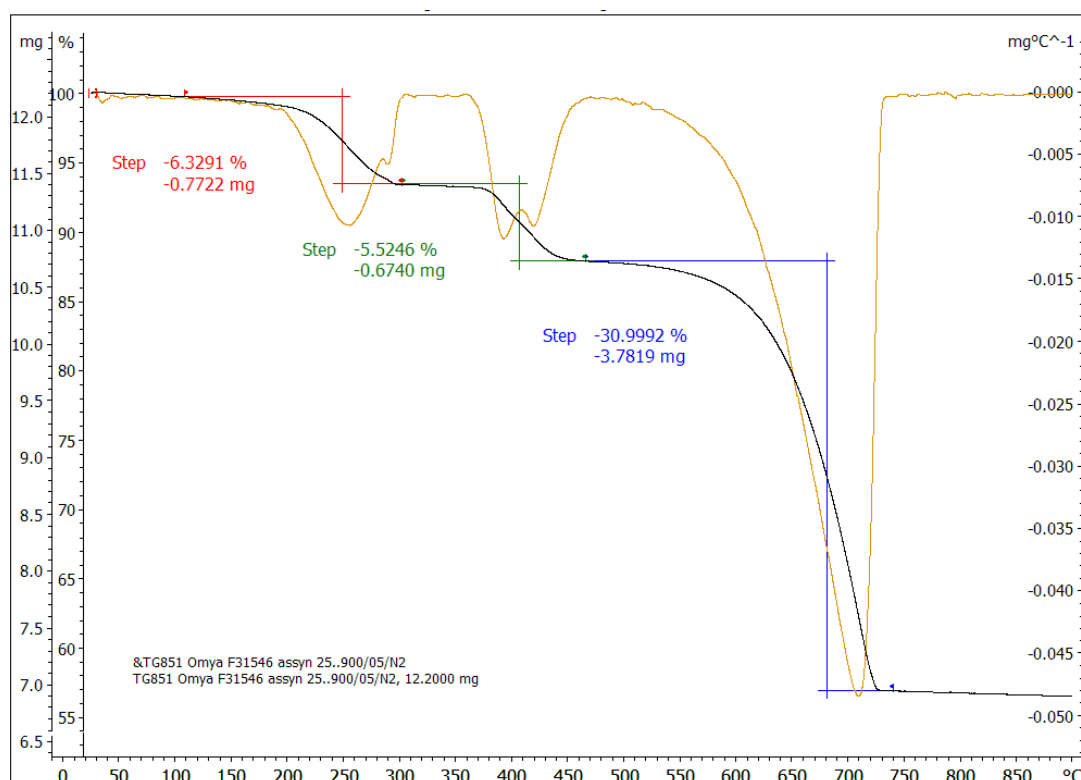
Figure 45: TG curve of BCC-syn (black) with first derivative (orange), weight losses of water (red, green) and CO_2 (blue)

This data were compared with literature values given by Matsushita et al. (1993, 1995), all are summarized in the Table 11. The theoretical amount of CO_2 and H_2O/OH of the literature formula as a 1.5-hydrate (Schimmel, 1970a,b) is also listed in this table.

T[°C]	comp.	TG obs	lit.(1993)	lit.(1995)	theor.
150 - 350	H_2O	6.7 %	6.5 %	6.3 %	14.9 %
350 - 500	H_2O	5.6 %	6.6 %	6.1 %	
500 - 775	CO_2	31.0 %	31.4 %	30.3 %	29.7 %

Table 11: Weight loss comparison for BCC to literature and theoretical data.

Because of the data from this study and the results reported by Matsushita et al. (1993, 1995) it can be concluded that the known BCC formula has to be corrected to $Ca_3(CO_3)_2(OH)_2 \cdot H_2O$, i.e. BCC-syn is the monohydrate form of calcium carbonate hydroxide hydrate with calculated values of -6.1, -6.1 and -30.6 wt% for H_2O, OH and CO_2, respectively. The molecular water content in literature is given from 1.5 H_2O (Schimmel, 1970) to $n H_2O$ (Matsushita et al., 1993). This discrepancy is unclear as all authors based their findings on TG-analyses.

5.4.2. Evolved gas mass spectrometry (TG-EGA-MS)
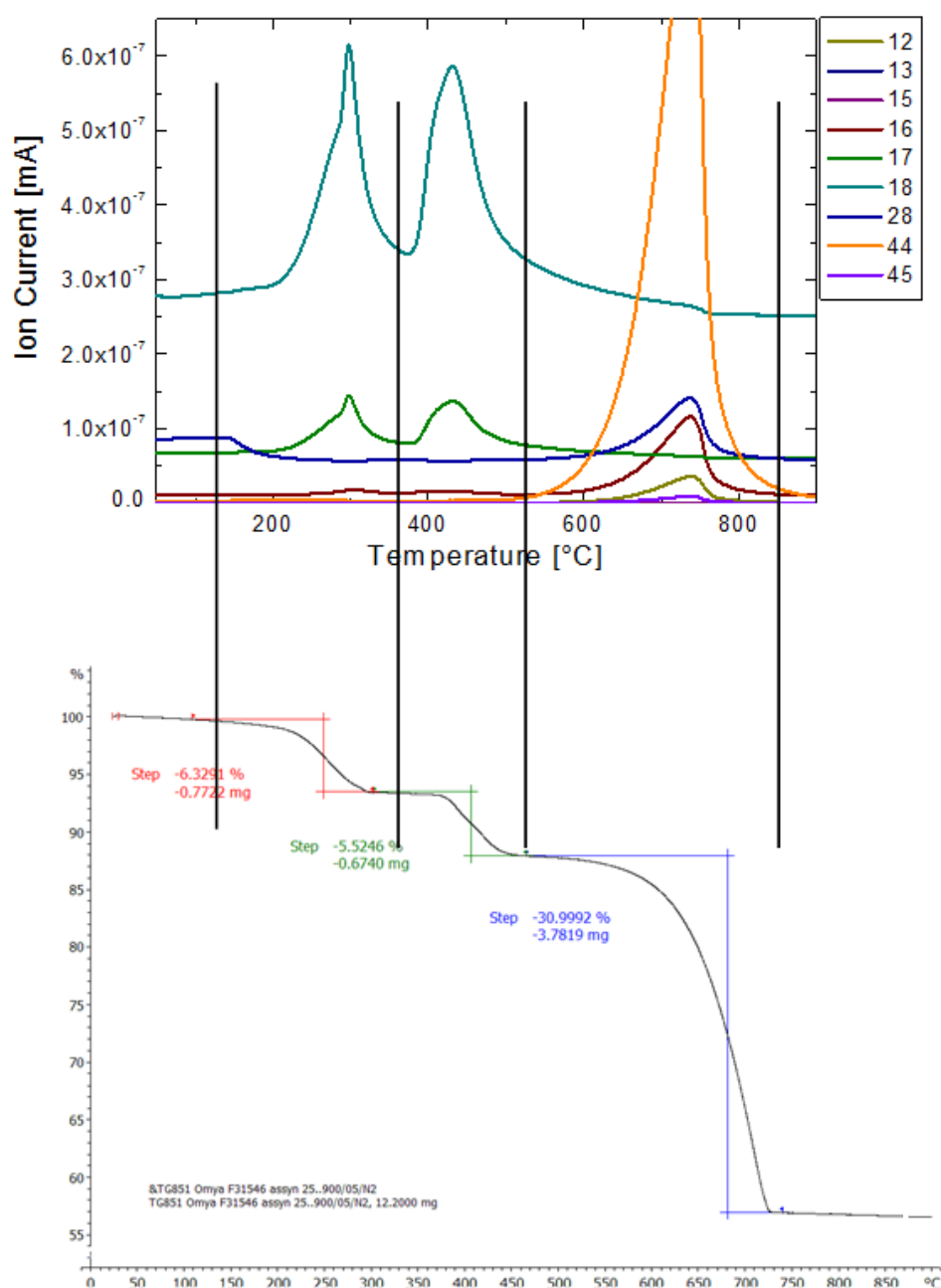
Figure 46: TG-MS curve vs. TG curve of BCC-syn

The TG-MS measurement under He also revealed an almost identical weight loss behavior. Between 150 and 500 °C there is a two-step loss (-6.3, -5.5 wt%) of water and between 500 and 900 °C the BCC-syn loses -31.0 wt% CO_2. In Figure 46 the EGA-MS curves are compared with the TG curve. The masses 12, 16, 28, **44** and 45 belong to the decomposition of carbon dioxide, while the masses 16, 17, **18** belong to the disintegration of water. Mass 15 can be attributed to CH_3^+ or NH^+. The plot clearly demonstrates the first two endothermic weight losses to be the results of dehydration/ dehydroxylation, whereas decarbonatization starts above 500 °C.

5.4.3. Differential scanning calorimetry (DSC)

An investigation of BCC-syn with the DSC was performed in a temperature range of 0 to 550 °C with a heating rate of 10 °Cmin^{-1}. The DSC curves are shown in Figure 47 with two endothermic processes at 200 and 425 °C. At a temperature of approximately 300 °C an exothermic process comes into effect. Matsushita et al. (1995) interpreted this process as the initial crystallization of calcite, which is not compatible to the results of the dT-pXRD measurements. A further measurement was recorded to compare the BCC-syn with the precipitate of the slurry. The two curves show no differences, except an additional endothermic process at 350 °C in BCC-slurry (Figure 48).
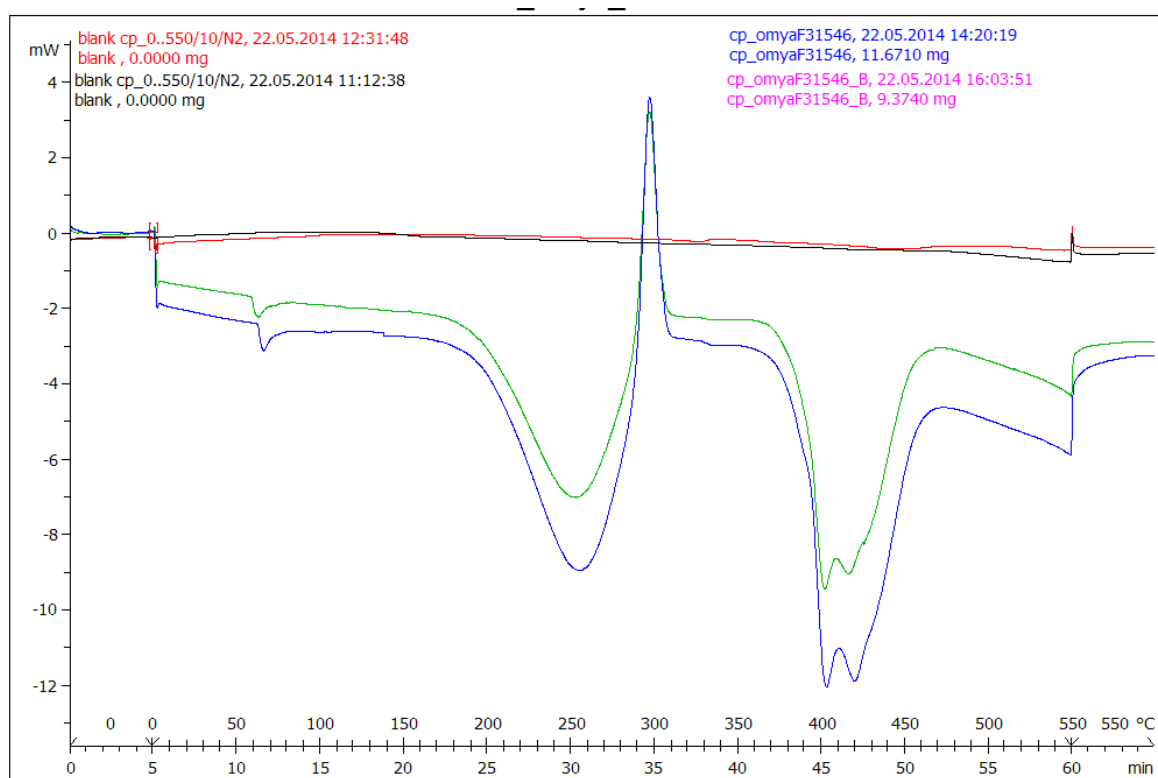
Figure 47: DSC curves of two BCC-syn (green, blue) and blank (black, red) measurements
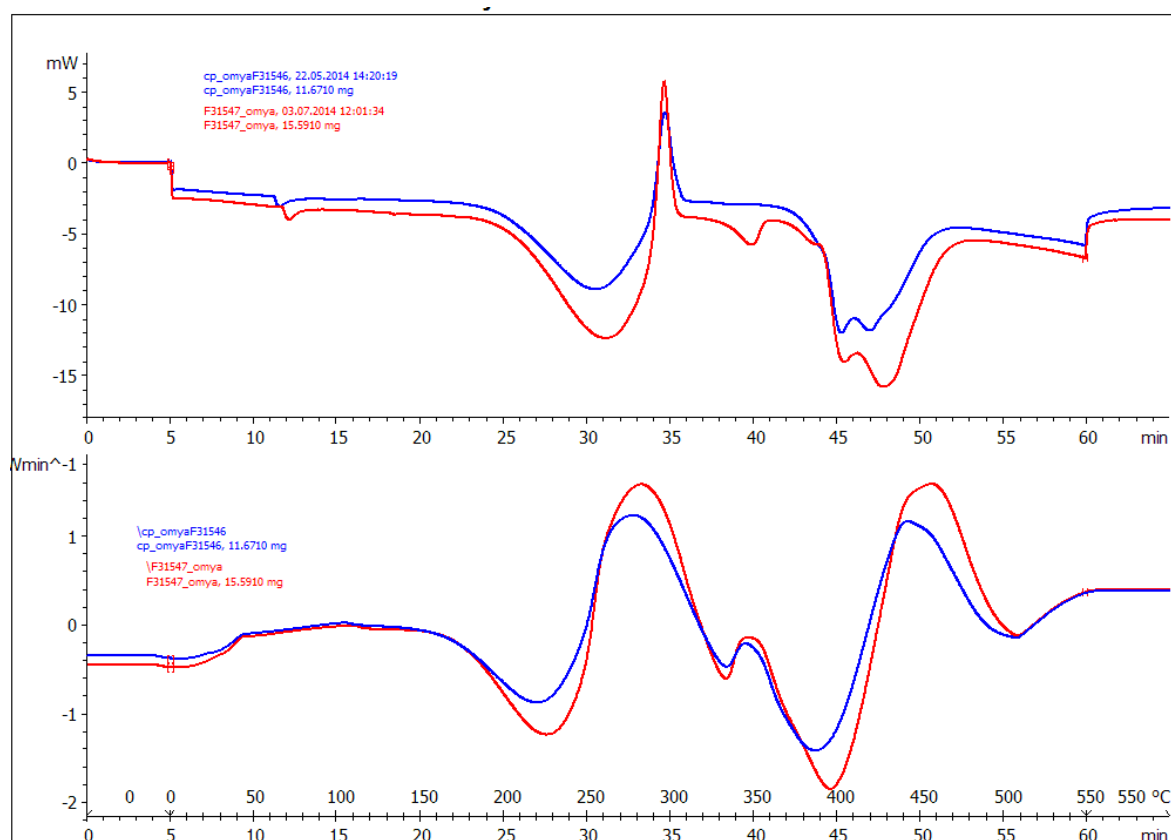
Figure 48: above: DSC curves of BCC-syn (blue) and BCC-slurry (red); below: first derivative of both samples.

5.5. CHNS-analysis

The chemical composition of the precipitated BCC-syn was also analyzed with an ELEMENTAR vario MACRO analyzer and in addition two measurements with a LECO RC612 instrument were performed. The results correspond with the TG findings and literature data. The results of the chemical analyses are given in Tables 12 and 13. The errors of the results from the MACRO analyzer were calculated by measuring 5 standards. These errors are correct for carbon. For hydrogen, nitrogen and sulfur a higher value must be assumed, because of the low content in the sample.

C	H	N	S
[wt%]	[wt%]	[wt%]	[wt%]
8.38(11)	0.97(10)	0.11(1)	0.38(1)

Table 12: CHNS content of BCC-syn from the MACRO analyzer.

The carbon amount can be converted to the carbon dioxide amount, which is 30.686 wt%.

C	CO_2
[wt%]	[wt%]
8.02(24)	29.37(88)
7.99(24)	29.31(88)

Table 13: CO_2 content of BCC-syn from the LECO RC612.

6. Discussion

The hitherto unknown structure of basic calcium carbonate (BCC) is the main topic of this thesis. As BCC is a precipitated calcium carbonate only powder material of poor crystallinity is available. This prevents a high-quality structure solution known from single-crystal materials. However, for a first approximation the obtained structure model for BCC is quite reasonable. There are many points open to discuss. The beta angle with 90.08° could be a hint that BCC exhibit orthorhombic symmetry. Further disagreements can be found at the seven coordinated calcium polyhedron and the associated edge-linked carbon groups. Contrary, the structure model of BCC has apparent similarities to the related mineral hydromagnesite, the starting material portlandite, and to the conversion product vaterite.

The second topic of this work was the characterization of the physicochemical properties of BCC. Due to the applied methods, a series of results were obtained. According to the observed and calculated weight losses for BCC and data from literature, one can state a mismatch with the reported chemical formula. As the observed weight loss is -12.3 wt%, which is very close to the calculated value for the monohydrate (-12.2 wt%) one can give the corrected chemical formula for BCC as $Ca_3(CO_3)_2(OH)_2 \cdot H_2O$.

Environmental stability is crucial for the application of BCC. The best conditions for the durable storage of BCC are dry settings. This is confirmed by pXRD analysis. At higher humidity conditions it transforms into vaterite-type calcium carbonate, while under a dry heating process it dehydrates and dehydroxylates to calcite-type calcium carbonate. Dehydrated BCC rehydrates not to BCC, it also changes to vaterite-type calcium carbonate. High quality SEM images of a rapid converted vaterite-type calcium carbonate reveal imperfect pseudomorphs of vaterite after platy BCC. The thermal stability of BCC is proven up to 150 or 175 °C under vacuum or dry He environments, respectively.

The title compound contains structurally different types of OH and CO_3-groups, whereas the nature of its water content is up to now not fully understood. This is indicated through the missing of the respective bending vibration in the IR data recordings. The existence of two types of bonded water entities, however, is obvious due to the distinct, step-type weight losses at two different temperatures (150-300 °C: -6.7 wt%; 350-500 °C: -5.6 wt%). These results were also proofed with TG-MS measurements, which showed that there is no difference in the evolved gas MS-spectra between dehydration (150-300 °C) and

dehydroxylation (350-500 °C). All temperature resolved analyses reveal the dehydroxylation to be a two-step process. The DSC data show three corresponding endothermic processes followed by a fourth one due to the release of CO_2 (500-750 °C: -31 wt%).

7. List of References

∇ AHN, J.W., JOO, S.M., KIM, H.S., KIM, D.H., KIM, J.P., KIM, H. (2003): Influence of final crystal with synthesis of basic calcium carbonate by carbonation process. Materials Science Forum, 439, 244-253.

∇ AHN, J., YOU, K., HAN, G., RYU, M., KIN, H. (2011): Method for manufacturing subsidence calcium carbonate via basic calcium carbonate and subsidence calcium carbonate manufactured with this. Patent application KR20110041198 (A), registered 21/04/2011, applicant: Korea Institutes of Geosciences and Mineral Resources.

∇ AKAO, M., IWAI, S.I. (1977): The hydrogen bonding of hydromagnesite. Acta Crystallographica, B33, 1273-1275.

∇ BRESE, N.E., O'KEEFFE, M. (1991): Bond-valence parameters for solids. Acta Crystallographica, B47, 192-197.

∇ BRUKER (2000): TOPAS, General profile and structure analysis software for powder diffraction data. Version 3, Bruker AXS, Karlsruhe, Germany.

∇ BRUKER (2005): Opus – Software for Bruker's Infrared and Raman Instruments – Version 5.5. Bruker Optics Inc., Ettlingen, Germany

∇ BRUKER (2007): DIFFRACplus Evaluation Package - EVA V13. Bruker AXS, Karlsruhe, Germany.

∇ CARACAS, R., BOBOCIOIU, E. (2011): The WURM project – a freely available web-based repository of computed physical data for minerals. American Mineralogist, 96, 437-443, *wurm.info*, ID: w000285, [access to web: 07/02/2014]

∇ CHEN, B.Z., JIANG, J.B., XU, H., SHI, X.C., WU, B.A. (2008): Preparation of basic magnesium carbonate by pyrogenation. Journal of Central South University (Science and Technology), 39 (5), 907-912.

∇ DOWTY, E. (2005): ATOMS – Shape Software – Version 6.3, Kingsport, Tennessee, USA

∇ FLEET, M.E. (1976): Distortion parameters for coordination polyhedra. Mineralogical Magazine, 40, 531-533.

∇ GRIFFITH W. P. (1970): Raman studies on rock forming minerals, Part II. Minerals containing MO_3, MO_4 and MO_6 groups. Journal of the Chemical Society A, 1970, 286-291.

∇ GROTHE, J. (1991): Verfahren zur Herstellung von basischen Kalziumkarbonat, danach hergestelltes basisches Kalziumkarbonat und seine Verwendung. Patent application 89122027.9, registered 29/11/1989, published 05/06/91, applicant: SCHAEFER KALK, Schaefer, J., Kalkwerke KG, Diez, Deutschland.

∇ KOICHI, T., TETSUO, K., KAZUO, Y. (1990): Production of cubic calcium carbonate having uniform particle diameter. Patent application 01-005387, registered 12/01/1989, published 19/07/90, applicant: Okutama Kogyo KK.

∇ LIU, X.W., FENG, Y.L., LI, H.R. (2011): Preparation of magnesium carbonate and its thermal decomposition kinetics in air. Journal of Central South University of Technology, 18, 1865 – 1870.

∇ MATSUSHITA, I., HAMADA, Y., SUZUKI, T., NOMURA, Y., MORIGA, T., ASHIDA, T., NAKABAYASHID, I. (1993a): Crystal structure of basic calcium carbonate and its decomposition process in water. Journal of the Ceramic Society of Japan, 101, 1335-1339.

∇ MATSUSHITA, I., NAKANISHI, J., KONG, T., MORIGA, T., ASHIDA, T., NAKABAYASHID, I. (1993b): Pyrolysis mechanism of basic calcium carbonate. Journal of the Ceramic Society of Japan, 101, 895-899.

∇ MATSUSHITA, I., NAKANISHI, J., KONO, T., SEKITA, T., MORIGA, T., ASHIDA, T., NAKABAYASHID, I. (1995): Effect of atmosphere on the pyrolysis process of basic calcium carbonate. Journal of the Ceramic Society of Japan, 103, 240-244.

∇ MEYER, H.J. (1960): Über Vaterit und seine Struktur. Fortschritte der Mineralogie. 38, 186-187.

∇ OriginLab (2002): Origin - Graphing and analysis - Version 6.1, OriginLab Corporation, Northampton, Massachusetts.

∇ PETCH, H.E. (1961): The hydrogen positions in portlandite, $Ca(OH)_2$, as indicated by the electron distribution. Acta Crystallographica, 14, 950-957.

∇ PFALLER, H., STRAUCH, D. (1997): Carbonate containing mineral fillers more particulary for use as matting agents. Patent application 437,638, registered 09/05/1995, published 03/06/97, applicant: Pluess-Staufer AG, Oftringen, Switzerland.

∇ PIETSCH, E., (1939): Gmelin's Handbuch der Anorganischen Chemie - Magnesium Teil B, Deutsche Chemische Gesellschaft, 8. Auflage, 321-330.

∇ PIETSCH, E., KOTOWSKI, A., (1939): Gmelin's Handbuch der Anorganischen Chemie - Calcium Teil B, Deutsche Chemische Gesellschaft, 8. Auflage, 956.

∇ RYU, M., YOU, K., AHN, J., KIM, H. (2007): Effect of the pH and basic additives on the precipitation of calcium carbonate during carbonation reaction. Resources Processing, 54, 14–18.

∇ RYUICHI, K., MITSUO, Y RYUICHI, K., MITSUO, Y. (1991): Coated paper for printing. Patent application 01-171672, registered 03/07/1989, published 21/02/91, applicant: Mitsubishi Paper Mills LTD.

∇ SATO, M., MATSUDA, S. (1969): Structure of vaterite and infrared spectra. Zeitschrift für Kristallographie, 129, 405-410.

∇ SCHIMMEL, G. (1970a): Basische Calciumkarbonate. Die Naturwissenschaften, 57 Jahrgang, 1, 38-39.

∇ SCHIMMEL G. (1970b): Elektronenmikroskopische Beobachtungen an basischen Calciumcarbonaten. Physikalische Blätter, 26/5, 213-216.

∇ SeaSolve (2003): PeakFit – Program for Peak Seperation and Analysis – Version 4.12, SeaSolve Software Inc., Framingham, MA

∇ TAS, A.C. (2008): Use of vaterite and calcite in forming calcium phosphate cement scaffolds. Ceramic Engineering and Science Proceedings, 28, 9; 135-150.

∇ TOMIZAWA, T., HARA, S., HASHIMOTO, H. (1976): Studies on the exothermic processes in the thermal decomposition of basic magnesium carbonate. Yogyo Kyokai-Shi, 84, 259-264.

∇ UTSUGI, H., ENDO, A., SUZUKI, N., HANAOKA, N., OSHIO, K., NAOI, T. (1982): Studies on pyrolysis and pyrolysis products of the basic magnesium carbonate. *https://www.cas.org/products/scifinder*, [acess to web: 03/06/2014].

∇ VAGENAS, N.V., GATSOULI, A., KONTOYANNIS, C.G. (2003): Quantitative analysis of synthetic calcium carbonate polymorphs using FT-IR spectroscopy. Talanta, 59, 831-836.

∇ WEIR, C.E., LIPPINCOTT, E.R. (1961): Infrared studies of aragonite, calcite, and vaterite type structures in the borates, carbonates, and nitrates. Journal of Research of the National Bureau of Standards-A: Physics and Chemistry, 65A, 3, 173-183.

∇ WILSON, A. J. C. (editor) (1992): International tables for crystallography, Vol. C. Kluver, Dordrecht, Netherlands.

∇ YAMADA, H., TSUNEMATSU, S., JINNAI, K. (1991): Production of basic calcium carbonate. Patent application 01-267835, registered 12/10/1989, published 29/05/91, applicant: Agency of Ind. Science & Technology.

8. List of Figures

9. List of Tables

10. List of Abbreviations

BCC   basic calcium carbonate
DTA   differential thermal analysis
DSC   differential scanning calorimetry
ICDD   International Centre for Diffraction Data
pXRD   powder X-ray diffraction
TA   thermal analysis
TG   thermogravimetry
SEM   scanning electron microscope
CHNS   Carbon, Hydrogen, Nitrogen, Sulfur Analysis
IR   infrared spectroscopy
TG-MS   thermogravimetry with mass spectrometry

11. Curriculum vitae

ING. MANUEL RIPKEN, BSC.

19/11/1988 ● Vienna

Mobile +43 (0) 676 / 47 74 616 ● m.ripken@gmail.com

EDUCATION

since (10/2013) – University of Vienna – Master of Science program in Earth sciences with main focus on mineralogy & crystallography

♦ Master thesis: *„Structural and physicochemical characterization of basic calcium carbonate (BCC)"*

- Ambient & non-ambient behavior
- Thermal analysis with TG, DSC and TG-MS
- Molecule spectroscopy: IR and Raman
- CHNS- and SEM analysis
- Structure determination powder diffraction

♦ Curriculum:

- Crystallography, crystal chemistry, crystal physics
- X-Ray diffraction methods, crystal structure analysis
- Mineralogy and mineral spectroscopy
- Scanning electron microscopy, electron probe micro analysis, ICP-MS, ICP-OES, RFA
- Thermal analysis: TG, DSC

(10/2010)-(11/2013) - University of Vienna – Bachelor of Science program in Earth sciences

♦ Bachelor thesis: „Heat capacity measurements of chosen minerals"

- Single crystal and powder measurements of quartz, periclase und corundum with DSC

♦ Curriculum:

- Mineralogy & Crystallography, material sciences,
- Sedimentology, structural geology, petrology, volcanology, geo chemistry, stratigraphy, paleobiodiversity

(09/2002)-(06/2008) - College of chemistry specializing in analytical chemistry – Environmental technology

♦ Theoretical focus: *„Current inventory of ore deposits in Austria and their usage"*

♦ Final project: *„Analysis of a plant-based raw material"*

WORK EXPERIENCE

since (05/2009) **(from (10/2010)** minor employment) -
Chemical-technical employee - ESW Consulting Wruss ZT GmbH

- Sample preparation
- Determination of PAH/PCB with GC-MS
- Determination of hydrocarbons with GC-FID
- Specialized analysis: Pesticides, phenols, heterocycles and organotin-compounds

(10/2013)-(01/2015) – **Teaching assistant in chemistry** – **University of Vienna**

- Stoichiometry and chemical calculations of solubility products, buffer systems, pH-values and thermodynamic systems

(07/2007) - **Internship**
Laboratory assistant – Messer Austria GmbH

- Quality control: Purity testing of gases

(07/2004) - **Internship**
Laboratory assistant – Wilhelminenspital, Laboratory

- Determination of medical parameters

SKILLS

IT & Software

- MS Office, Origin 6.1, Sigma Plot 12, Atoms 63, EVA V13

Languages

- German, English

AWARDS AND FINANCIAL SUPPORT

(10/2013)-(10/2014) – Merit-based scholarship of the University of Vienna

(10/2012)-(10/2013) – Merit-based scholarship of the University of Vienna

(10/2011)-(10/2012) – Merit-based scholarship of the University of Vienna

REFERENCES

Ao.Univ-Prof. Dr.Christian L. Lengauer
University of Vienna – Institute of Mineralogy & Crystallography
Althanstraße 14 (UZA 2), 1090 Vienna, Austria
M:(+431) 4277 53243   E: christian.lengauer@univie.ac.at

Dipl.-Ing. Oliver Mann
ESW Consulting Wruss ZT GmbH
Rosasgasse 25-27, 1120 Vienna, Austria
M:(+431) 8125318 320   E: oliver.mann@wruss.at

Vienna, 23/04/15   (Ing. Manuel Ripken, BSc)